THE RELATIONSHIP BETWEEN FNWC SURFACE WIND ANALYSIS AND NOAA/NESS GOSSTCOMP (SST) DATA IN THE EASTERN SOUTH PACIFIC

George Hamilton Berry

NAVAL POSTGRADUATE SCHOOL
Monterey, California
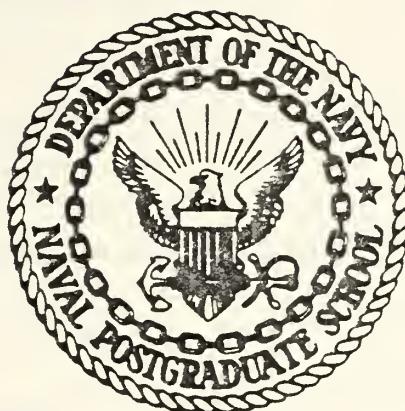
THESIS

THE RELATIONSHIP BETWEEN FNWC SURFACE
WIND ANALYSIS AND NOAA/NESS GOSSTCOMP (SST)
DATA IN THE EASTERN SOUTH PACIFIC

by

George Hamilton Berry

June 1977

Thesis Advisor: R. L. Haney
Thesis Advisor: J. B. Wickham

T178621+2

REPORT DOCUMENTATION PAGE		READ INSTRUCTIONS BEFORE COMPLETING FORM
1. REPORT NUMBER	2. GOVT ACCESSION NO.	3. RECIPIENT'S CATALOG NUMBER
4. TITLE (and Subtitle) The Relationship between FNWC Surface Wind Analysis and NOAA/NESS GOSSTCOMP (SST) Data in the Eastern South Pacific		5. TYPE OF REPORT & PERIOD COVERED Master's Thesis; June 1977
		6. PERFORMING ORG. REPORT NUMBER
7. AUTHOR(s) George Hamilton Berry		8. CONTRACT OR GRANT NUMBER(s)
9. PERFORMING ORGANIZATION NAME AND ADDRESS Naval Postgraduate School Monterey, California 93940		10. PROGRAM ELEMENT, PROJECT, TASK AREA & WORK UNIT NUMBERS
11. CONTROLLING OFFICE NAME AND ADDRESS Naval Postgraduate School Monterey, California 93940		12. REPORT DATE June 1977
		13. NUMBER OF PAGES 65
14. MONITORING AGENCY NAME & ADDRESS(if different from Controlling Office) Naval Postgraduate School Monterey, California 93940		15. SECURITY CLASS. (of this report) Unclassified
		15a. DECLASSIFICATION/DOWNGRADING SCHEDULE

16. DISTRIBUTION STATEMENT (of this Report)

Approved for public release; distribution unlimited.

17. DISTRIBUTION STATEMENT (of the abstract entered in Block 20, if different from Report)

18. SUPPLEMENTARY NOTES

19. KEY WORDS (Continue on reverse side if necessary and identify by block number)

20. ABSTRACT (Continue on reverse side if necessary and identify by block number)

Sea surface temperature (SST) anomalies on the daily synoptic time scale from National Oceanic and Atmospheric Administration/National Environmental Satellite Service (NOAA/NESS) Global Operational SST Computationa (GOSSTCOMP) data in the Eastern South Pacific are compared to deviations of similar time scale from the means of both the wind stress curl and the friction velocity cubed as derived from Fleet Numerical Weather Central's (FNWC) mercator global band surface wind field.

DD $_{1\ JAN\ 73}^{FORM}$ 1473 EDITION OF 1 NOV 65 IS OBSOLETE
(Page 1) S/N 0102-014-6601 |

Example patterns of those variables as well as mean and unaltered fields are presented here. High correlations between the sea surface temperature deviations and the deviations of wind stress curl and friction velocity cubed were not attained at any log, owing largely to the paucity and poor quality of surface wind and satellite data. Further investigation is needed.

The Relationship between FNWC Surface
Wind Analysis and NOAA/NESS GOSSTCOMP (SST)
Data in the Eastern South Pacific

by

George Hamilton Berry
Lieutenant, United States Navy
B.S., University of Utah, 1972

Submitted in partial fulfillment of the
requirements for the degree of

MASTER OF SCIENCE IN METEOROLOGY AND OCEANOGRAPHY

from the
NAVAL POSTGRADUATE SCHOOL
June 1977

ABSTRACT

Sea surface temperature (SST) anomalies on the daily synoptic time
scale from National Oceanic and Atmospheric Administration/National
Environmental Satellite Service (NOAA/NESS) Global Operational SST Com-
putation (GOSSTCOMP) data in the Eastern South Pacific are compared to
deviations of similar time scale from the means of both the wind stress
curl and the friction velocity cubed as derived from Fleet Numerical
Weather Central's (FNWC) mercator global band surface wind field.
Example patterns of those variables as well as mean and unaltered fields
are presented here. High correlations between the sea surface tempera-
ture deviations and the deviations of wind stress curl and friction
velocity cubed were not attained at any log, owing largely to the
paucity and poor quality of surface wind and satellite data. Further
investigation is needed.

TABLE OF CONTENTS

LIST OF TABLES

LIST OF FIGURES

7

LIST OF SYMBOLS

C_d = drag coefficient

$\text{curl}_z \tau$ = vertical component of the curl of Tau

C_v = specific heat at constant volume

f = coriolis factor

$\dot{H}$ = rate of heating per unit mass

P = pressure

$\dot{Q}$ = rate of heating per unit volume

$R(z)$ = absorption of solar radiation in the sea

T = ocean temperature

T_s = surface ocean temperature

U_* = friction velocity

U = west-east component of wind vector

v = south-north component of wind vector

$\vec{V}$ = surface wind vector

$\overline{W_e}$ = mean Ekman vertical velocity

ρ_{wo} = density of ocean water at surface

$\rho_{wo} C_v (\overline{W'T'})$ = upward turbulent heat flux

ϕ = latitude

$\vec{\tau}$ = wind stress vector

τ_x = west-east component of the wind stress vector

τ_y = south-north component of the wind stress vector

9

ACKNOWLEDGMENTS

I. INTRODUCTION

The meteorological and oceanographic activity of the Southern Hemisphere, although not nearly as widely studied as that of the Northern Hemisphere, is still of vital importance to the United States and the rest of the world. Its cause-and-effect impact on the weather and ocean situations of the North, as well as on vast resources there not well utilized, arouses scientific curiosity to understand the physical processes in the region.

One facet of these activities which is of particular interest is sea surface temperature (SST). This paper will attempt to determine if weekly averaged non-seasonal fluctuations of wind phenomena analyzed by Fleet Numerical Weather Central (FNWC) can be correlated with non-seasonal fluctuations of sea surface temperatures revealed by Global Operational SST Computation (GOSSTCOMP) data. The major eventual goal is to examine mechanisms responsible for synoptic scale fluctuations in SST. If changes in wind phenomena can be related to the changes in SST, then temperature inferred from wind fields may serve as a substitute for satellite data and possibly for prediction purposes.

The specific area studied for this report was the Eastern South Pacific, off the coasts of Ecuador, Peru, and Chile.

The wind phenomena chosen for correlation were perturbations of the vertical component of the curl of the wind stress ($\text{curl}_z\tau$) and friction velocity cubed (U_*^3). (Symbols used in this thesis are defined on the List of Symbols on page 9.) These parameters were used because the curl of Tau is responsible for Ekman convergence and divergence, and

frictional velocity is related to mixing. Both of these can be found to contribute to SST changes.

Meridional Ekman advection (as represented by Tau_x) could also be studied for relationship with SST, but it was not found to be practical with data used in this paper.

II. DEVELOPMENT OF BASIC THEORY INVOLVING U_*^3, CURL OF TAU, AND SST

Starting with the first law of thermodynamics,

1. $C_v \dfrac{dT}{dt} + P \dfrac{d\alpha}{dt} = \dot{H}$, where $\dot{H}$ is the rate of heating per unit mass.

Assuming incompressibility, then

$$\frac{d\alpha}{dt} = 0 \ .$$

By expanding the total derivative of T and averaging it, while

neglecting $\vec{V} \cdot \nabla_2 \bar{T}$ and $\nabla_2 \cdot (\overline{V'T})$ (horizontal derivatives), we get

2. $\dfrac{\partial \bar{T}}{\partial t} + \overline{W_e} \dfrac{\partial \bar{T}}{\partial z} + \dfrac{\partial}{\partial z} (\overline{W'T'}) = \dot{Q}/\rho_{wo} C_v = R(z)$,

where R(z) is the absorption of solar radiation in the sea,

let $\dot{H} = \dot{Q}/\rho_{wo}$, and $\overline{W'T'}$ is proportional to the upward flux.

If we look at the mixed layer only, $\dfrac{\partial \bar{T}}{\partial z} = 0$, $\bar{T} = T_s$, and so (2)

becomes

3. $\dfrac{\partial T_s}{\partial t} + \dfrac{\partial}{\partial z} (\overline{W'T'}) = R(z)$ with $z > -h$.

Next integrate equation 3 in depth from the surface to z = -h and

neglect R(z), then

4. $\displaystyle\int_{-h}^{o} \dfrac{\partial T_s}{\partial t} \, dz = -[(\overline{W'T'})_o - (\overline{W'T'})_{-h}]$ which leads to

5. $\displaystyle\int_{-h}^{o} \dfrac{\partial T_s}{\partial t} = -(\overline{W'T'})_o + (\overline{W'T'})_{-h}$

Then with strong winds it would be expected that $(\overline{W'T'})_o$ (which is pro-

portional to U_* multiplied by the air sea temperature difference) be

larger and $(\overline{W'T'})_{-h}$ (which is proportional to U_*^3) be more negative

(Figure I). Thus, enhanced upward flux at the surface and downward flux

at -h would result in lowering the SST.
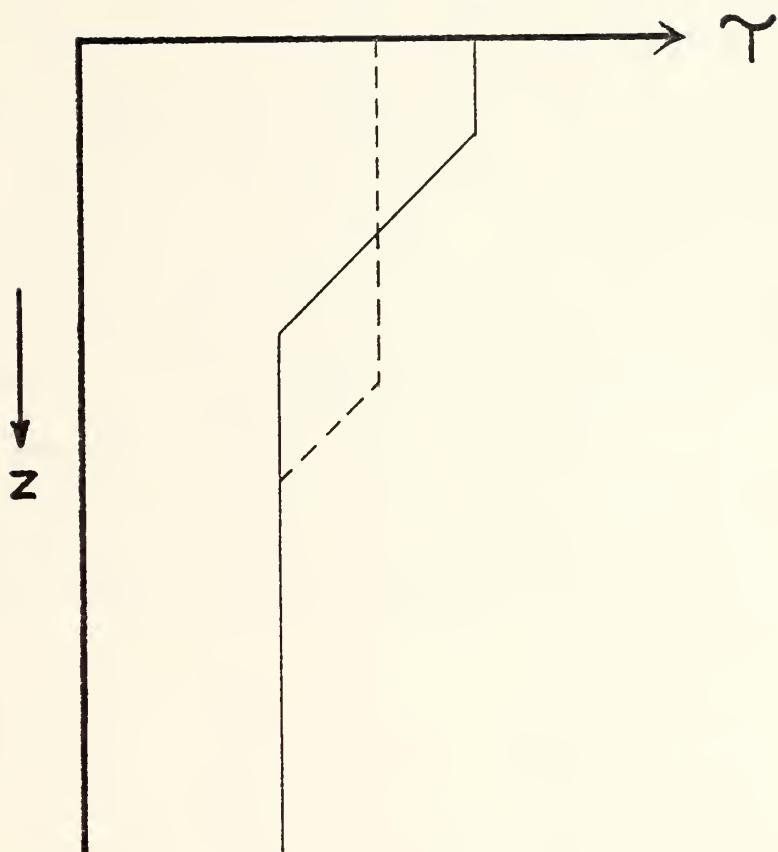
Figure 1. Influence of wind stress (τ) on ocean temperature (T) structure with depth. Solid line represents structure before U_* changed mixed layer. Dashed line represents resulting temperature profile after being effected by strong wind stress. Note how the mixed layer has lowered the surface temperature and increased the depth of the mixed layer.

In the equation (2) if $\frac{\partial \bar{T}}{\partial t}$ is not zero, there will be an effect of vertical advection. $\overline{W_e}$ is the mean vertical Ekman velocity and is directly related to the vertical component of the $\text{curl}_z \tau$.

6. $\overline{W_e} = \frac{1}{\rho_w f} \text{curl}_z \bar{\tau}$

In the Southern Hemisphere f is negative, and therefore, the current is directed 90° to the left of the wind. Also in the Southern Hemisphere where the winds in highs and lows rotate in opposite directions to that of the Northern Hemisphere, there is horizontal Ekman convergence and sinking motion within a surface counter-clockwise circulation and horizontal Ekman divergence and rising motion within a surface clockwise circulation. With this convergence, associated warming should be expected when the sign of $\text{curl}_z \tau$ is positive. Conversely clockwise circulation should have divergence yielding cooling with curl of Tau being negative. This process of surface diverging (converging) producing cooler (warmer) water has been called Ekman pumping (Figure 2).

The purpose of this thesis was to try to detect wind mixing (U_*^3) and/or Ekman pumping $(\text{curl}_z \tau)$ from FNWC wind data and the GOSSTCOMP data.
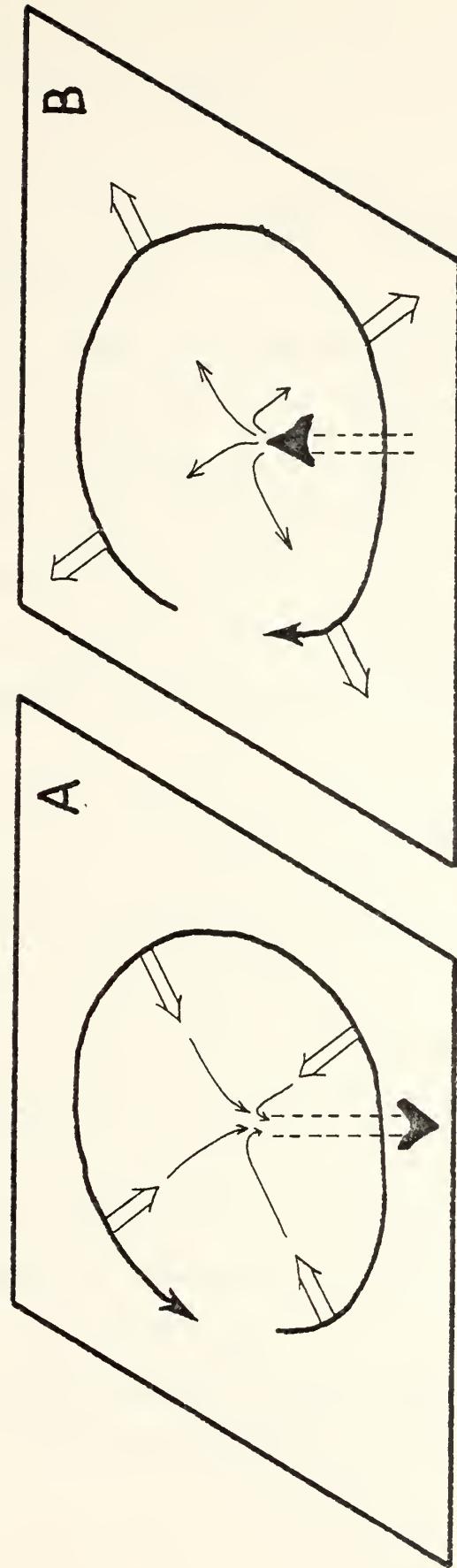
Figure 2. Diagram of the curl$_z$ τ in the Southern Hemisphere

A. Counter clockwise circulation of the wind produces convergence; hence downwelling of the water (dashed arrow) resulting in sea surface warming.

B. Clockwise circulation of the wind produces divergence; hence upwelling of the water (dashed arrow) resulting in sea surface cooling.

16

III. DATA

Sea surface temperature observations were obtained from National Oceanic and Atmospheric Administration/National Environmental Satellite Service (NOAA/NESS)'s GOSSTCOMP datum.

The GOSSTCOMP data was a NOAA satellite scanning radiometer product which had been modified and composited in time. A detailed description of this product is found in NOAA/NESS Technical Memorandum #78, June '76. During the time frame of this report, past SST information (climatology) was used as one type of validity check.

This data was supplied weekly by NOAA/NESS through Defense Mapping Agency--Inter-American Geodetic Survey (DMA-IAGS), Canal Zone, on computer print-out paper.

The area of interest was from the coast of South America to 100°West longitude, and from the Equator to 40° South latitude. SST was displayed in tenths of a degree every one-half degree of latitude and longitude along with a confidence factor for that area.

For the purpose of the study, SST's were picked manually every 2 1/2° latitude and longitude in order to smooth the field, to relate it to wind data at every 2 1/2°, and, finally, to allow a reasonable time in card punching for computer graphics. Thus a SST field covering the area studied was produced for a period beginning 22 May 1974 and ending 28 May 1975, with a total of 53 maps.

Marine surface wind observations came from FNWC global band mercator maps. This data covered the Northern Hemisphere up to 60° North and the

Southern Hemisphere to approximately 40° South. Every 12 hours wind

fields of surface "u" component and "v" component of wind in centimeters

per second for the time frame of the report were made available in tape

form for this study courtesy of FNWC. (Thesis data available from

J. B. Wickham, Department of Oceanography, NPS).

The winds andtemperatures were defined at grid points which were

equally spaced on the mercator projection and had to be converted to an

equally spaced latitude-longitude (2 1/2°) grid. To do this, FNWC's

Bessel interpolation scheme was used.

For the purpose of comparison, mean monthly SST maps came from

Fishing Information (1974-1975), a publication of National Marine

Fisheries Service (NMFS). Furthermore, the NMFS also supplied data

from the El Niño Watch Cruise (11 February 1975 to 27 May 1975).

IV. PROCESSING OF DATA

Using the wind field tapes supplied by FNWC, the wind stress ($\vec{\tau}$) was calculated by the following equation, which involved two assumed constants,

7. $\vec{\tau} = \overrightarrow{tau} = \rho_a C_d \, |V| \, \vec{V}$.

For practical use this can be separated into components

$$\tau_x = \rho_a \, C_d \, (u^2 + v^2)^{1/2} \, u \quad \text{and}$$

$$\tau_y = \rho_a \, C_d \, (u^2 + v^2)^{1/2} \, v \, ,$$

where the density of air, ρ_a , is .00122 gm/cm^3, and the drag coefficient, C_d , is .0013.

The τ_x and τ_y fields were calculated every 12 hours and then averaged for seven days. The last date used in calculating the average corresponded to a given SST data date.

The main interest in this data was to be able to calculate the mean vertical component of the curl of Tau and mean U_*^3. It is believed that the changes in SST can be related by equation 2, as noted in another section

2. $\dfrac{\partial \overline{T}}{\partial t} = - \, \overline{W}_e \, \dfrac{\partial \overline{T}}{\partial z} - \dfrac{\partial}{\partial z} \, (\overline{W'T'})$

    (1)   (2)   (3)

where term 1 is the change of mean temperature with time, term 2 is proportional to the curl of Tau, and term 3 is proportional to wind mixing.

The definition of friction velocity is

8. $U_* = (\frac{|\vec{\tau}|}{\rho_a})^{1/2}$ (Glossary of Meteorology, 1959)

which leads to

9. $\bar{U}_*^3 = \left(\frac{(\bar{\tau}_x^2 + \bar{\tau}_y^2)^{1/2}}{\rho_a}\right)^{3/2}$.

The finite difference form of the vertical component curl of Tau equation
in spherical coordinates over a seven day average is

10.

$$\vec{k} \cdot (\nabla \times \bar{\vec{\tau}}_{ij}) = \frac{1}{R\cos\phi_{ij}} \left[\left(\frac{\bar{\tau}_{yi+1,j} - \bar{\tau}_{yi-1,j}}{2\Delta\lambda}\right) - \left(\frac{(\bar{\tau}_x\cos\phi)_{i,j+1} - (\bar{\tau}_x\cos\phi)_{i,j-1}}{2\Delta\phi}\right)\right]$$

R   is the radius of earth in centimeters.

$\Delta\lambda$ and $\Delta\phi$ equals the grid spacing which is 2 1/2° converted to radians.

ϕ is the latitude in radians.

$\bar{\tau}_x$ is the west to east component of wind stress averaged over a

seven day period.

$\bar{\tau}_y$ is the south to north component of wind stress averaged over a

seven day period.

$\vec{k}$ The vector $\vec{k}$ is a unit vector directed vertically.

These equations were incorporated into an existing program for cal-
culating mean $\bar{\tau}_x$'s and $\bar{\tau}_y$'s. The results indicated that the curl Tau was
of the magnitude 10^{-7} -- 10^{-8} dyne/cm^3, comparable to that of Hantel
(1970), which was 2.3×10^{-8} dyne/cm^3, and the cube of the friction
velocity (U_*^3) was of the magnitude of 1×10^4 (cm/sec)^3.

The next step was to separate these seven day averaged fields into
mean and perturbation values for the purpose of removing the seasonal

20

cycle. Using the basic equation $A = \bar{A} + A'$ where $\bar{A}$ is the mean and
A' is the deviation of A from the mean, the weakly mean field was
used to develop the annual mean field of each parameter (Figures 3, 4,
5). Once mean fields were generated, they were subtracted from the
original field as shown by equations below

(with: i = number of days in a week and
j = number of weeks in a year)

$$(\text{curl}_z \, \tau)' = \text{curl}_z \, \tau - \left[\frac{1}{52} \sum_{j=1}^{52} \left(\frac{1}{7} \sum_{i=1}^{7} (\text{curl}_z \, \tau)_i\right)_j\right]$$

$$(\text{curl}_z \, \tau)' = \text{curl}_z \, \tau - \overline{\text{curl}_z \, \tau}$$

$$(U_*^3)' = U_*^3 - \left[\frac{1}{52} \sum_{j=1}^{52} \left(\frac{1}{7} \sum_{i=1}^{7} (U_*^3)_i\right)_j\right]$$

$$SST' = SST - \left[\frac{1}{52} \sum_{j=1}^{52} (SST)_j\right]$$

$$SST' = SST - \overline{SST}$$

The perturbation fields of the $\text{curl}_z \, \tau$, friction velocity cubed,
and sea surface temperature were put into contoured map form so that
their spatial variations could be examined. From an examination of these
maps a decision was made to concentrate the study on the mid-latitude
regions. A line of data from 27.5° South to 39.5° South at 87.5° West
was chosen because it was thought to be far enough from the coast to
eliminate coastal effects and close enough at mid-latitude to be under
the effect of mid-latitude storms.

On this North-South line, consisting of five stations (Figure 6)
separated by 2 1/2° latitude, the seven-day average SST's were plotted
for May 1974 to May 1975 (Figures 7A, 8A, 9A). A definite sinusoidal

21
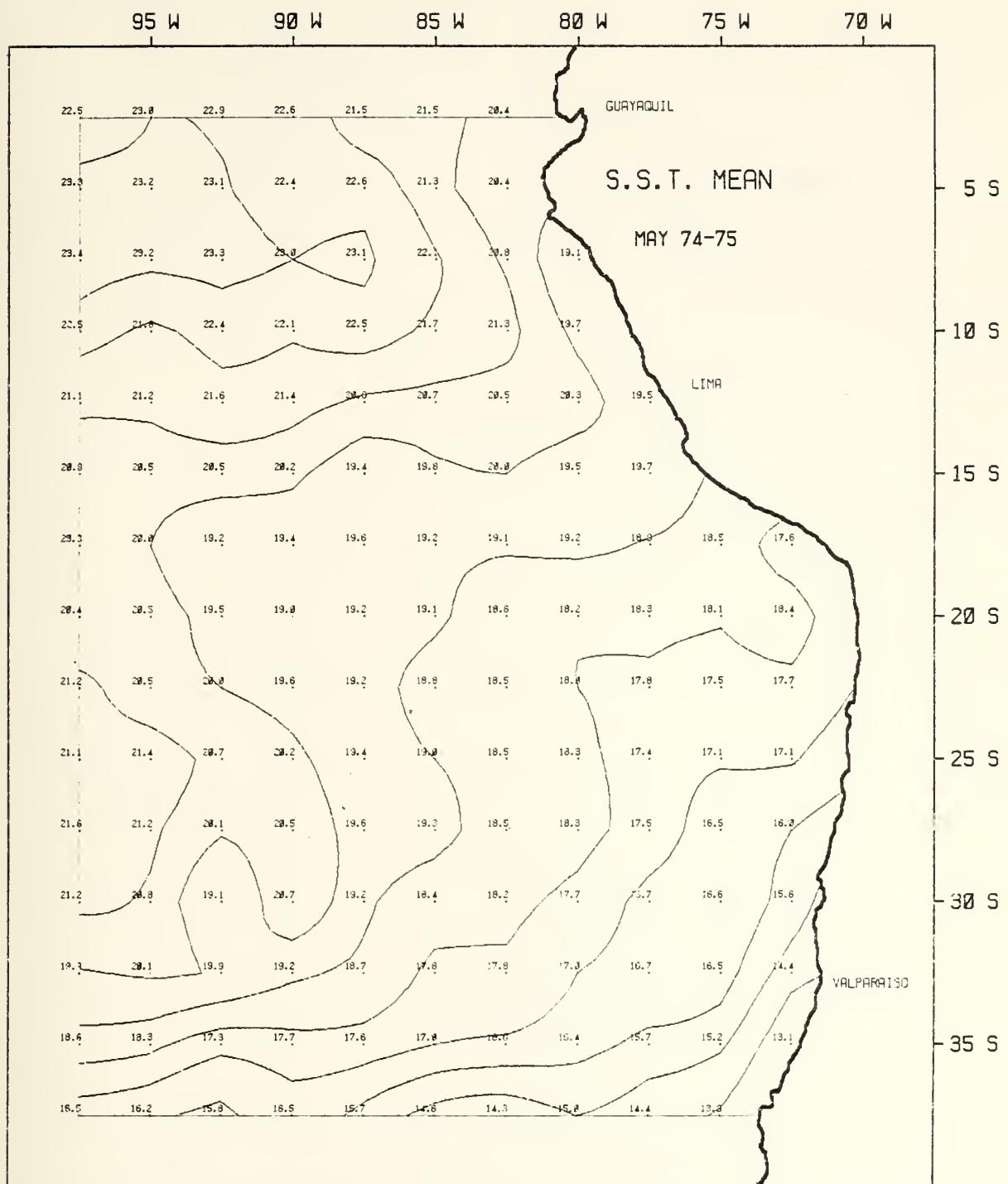
Figure 3.   Annual mean sea surface temperatures (°C) from 28 May 74
to 28 May 75.
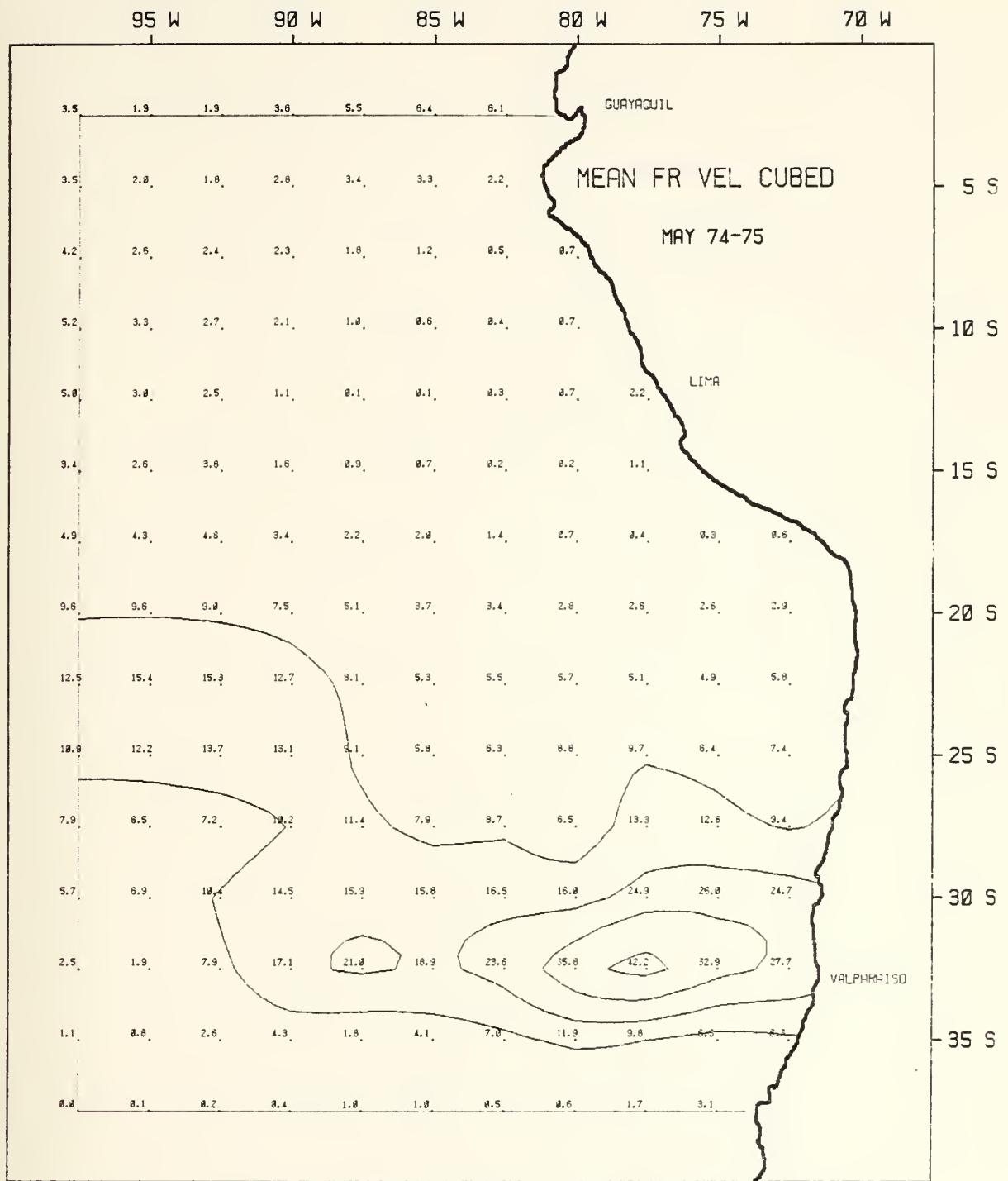
Figure 4.   Annual mean friction velocity cubed in 10^3 cm/sec from
            28 May 74 to 28 May 75.
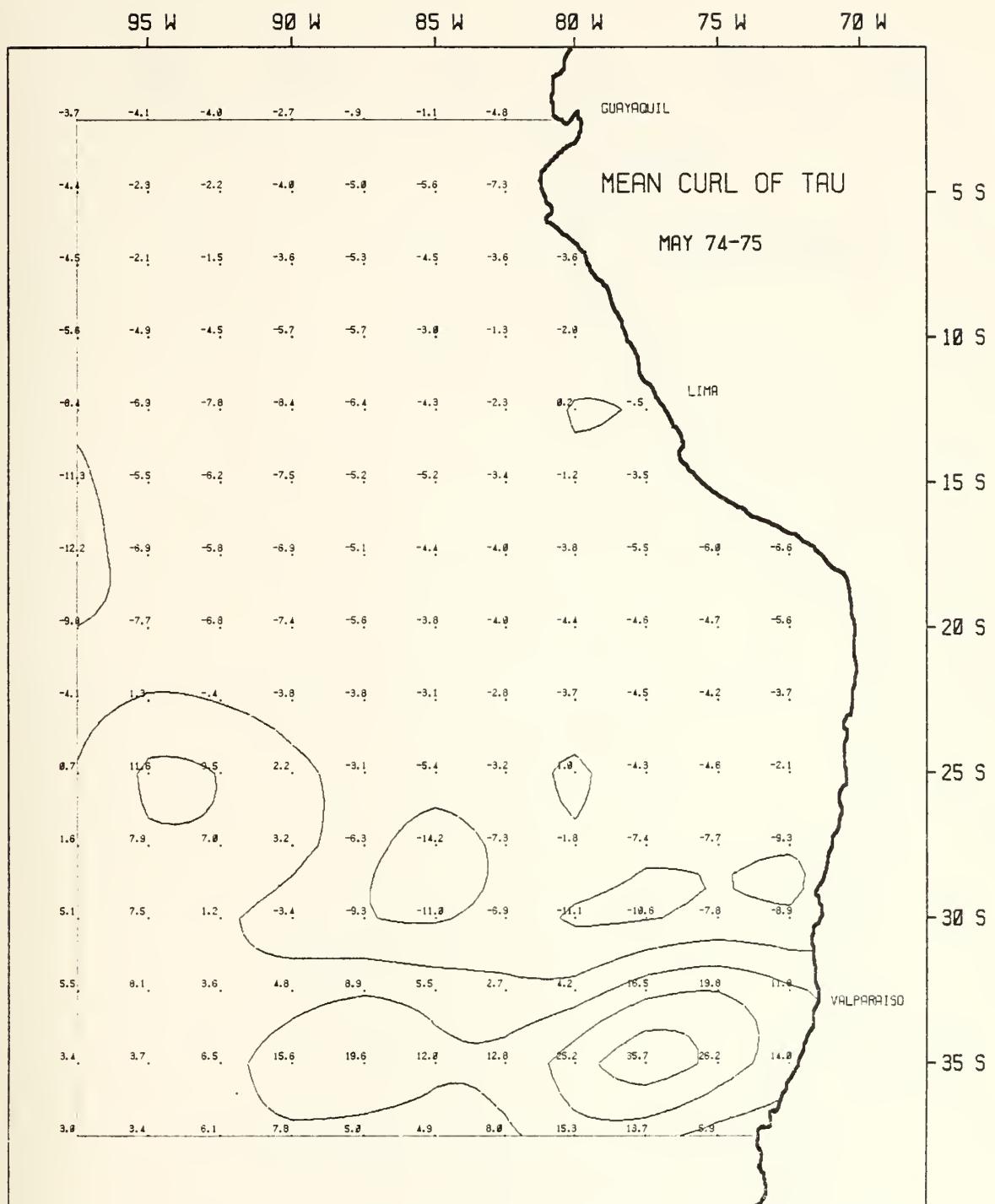
Figure 5. Annual mean curl$_z$ τ in 10^{-9} dyne/cm^3 from 28 May 74 to 28 May 75.
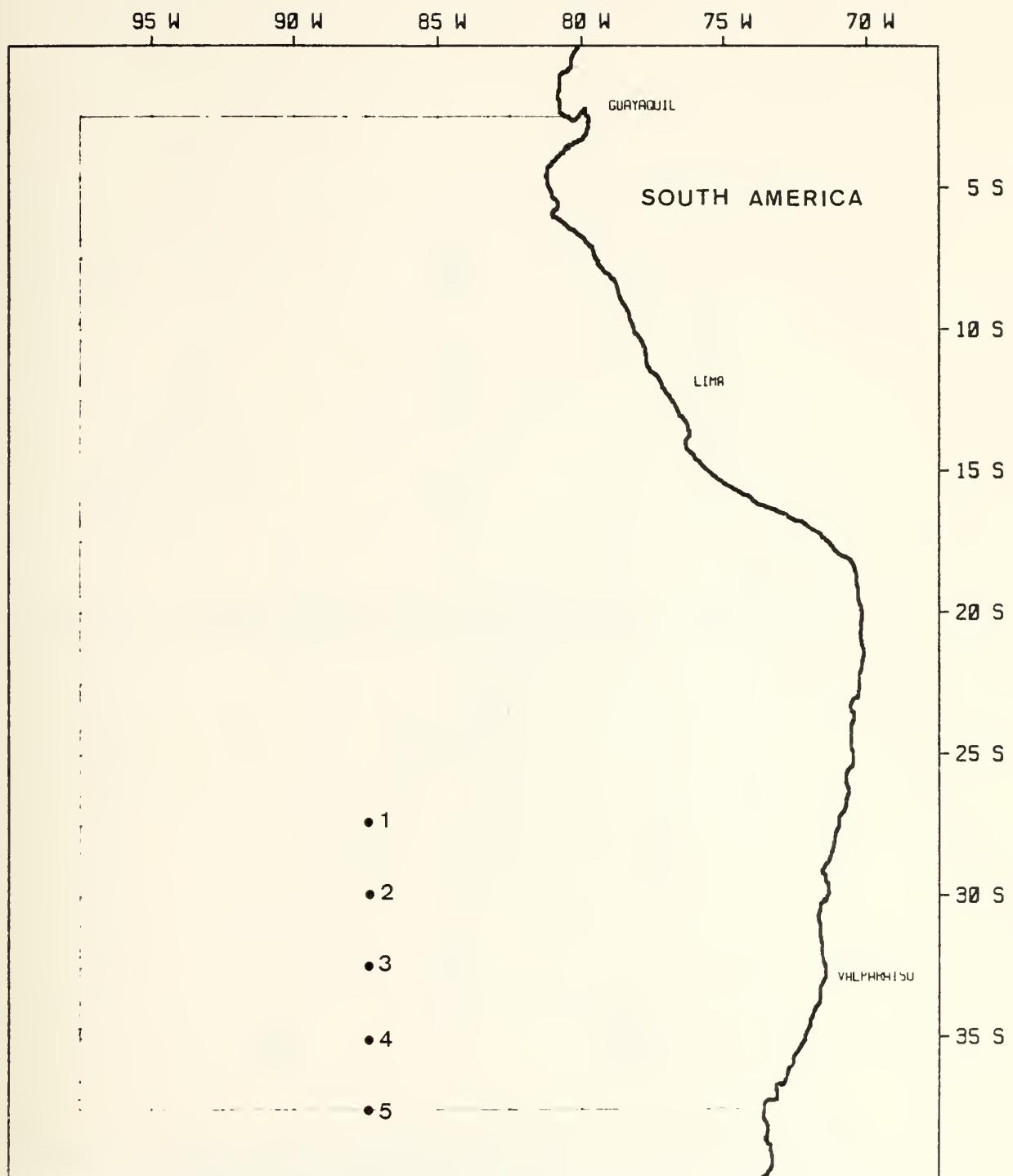
Figure 6. Location of the five sample points.
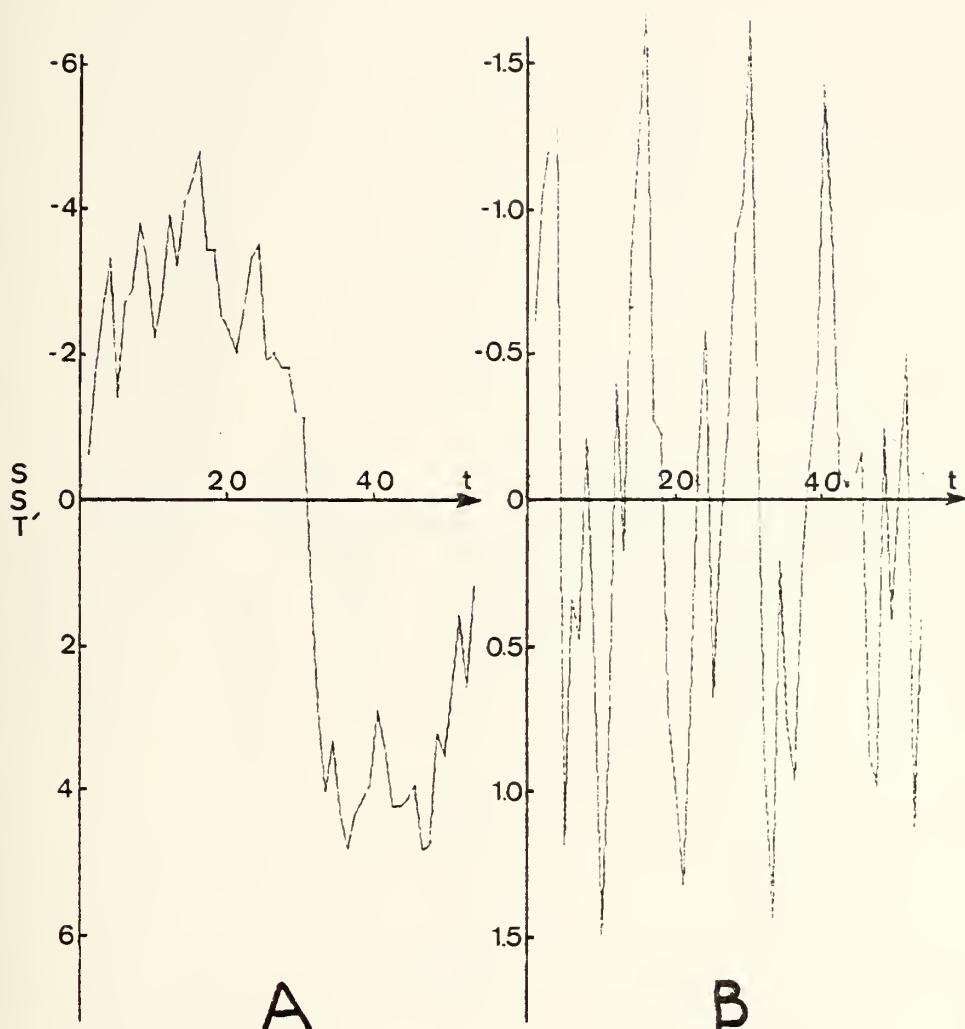
Figure 7. Weekly time (t) series for SST' for May 74 - May 75 at
32.5°N and 87.5°W (Station #3)
A. Represents the annual mean removed
B. Represents the seasonal cycle removed.
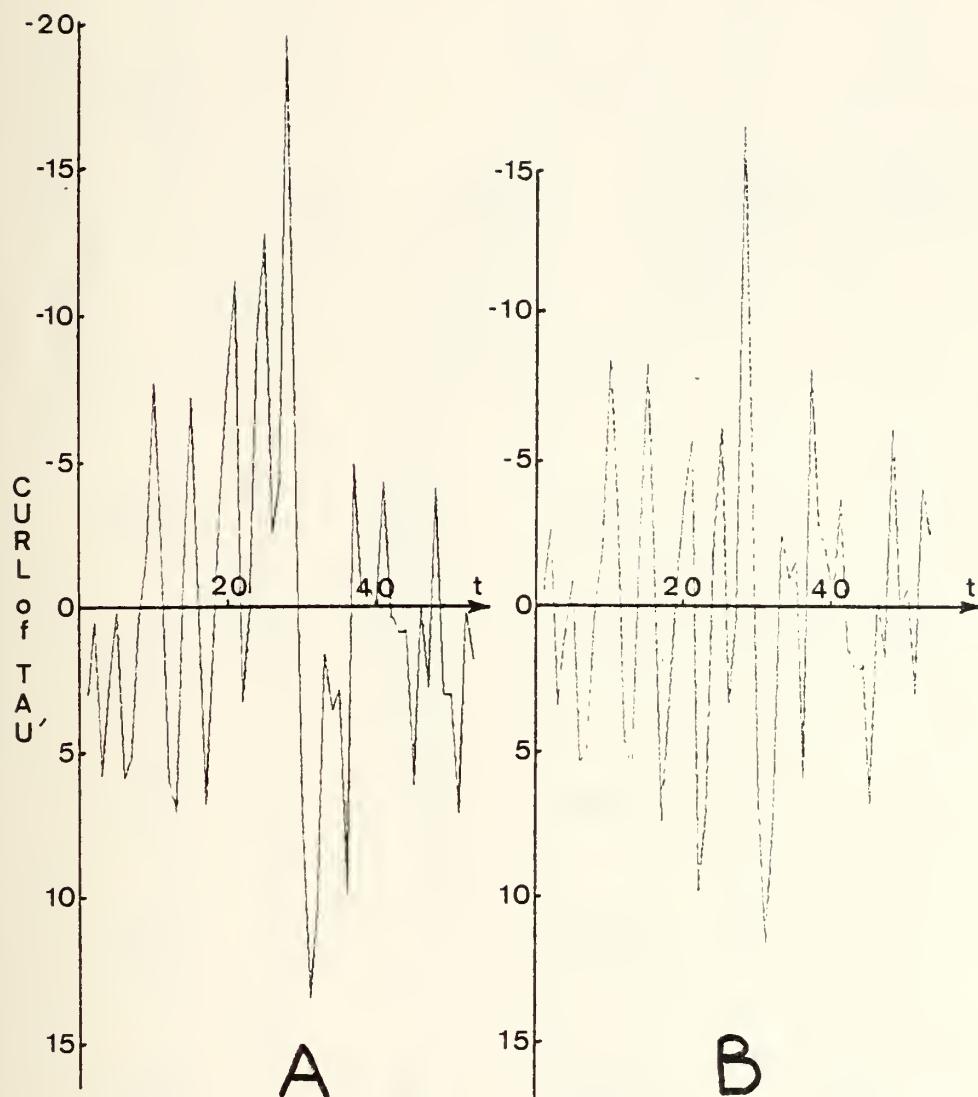
Figure 8. Weekly time (t) series for (curl$_z$ τ)' for May 74 - May 75 at 32.5°N and 87.5°W (Station #3)
   A. Represents the annual mean removed
   B. Represents the seasonal cycle removed.
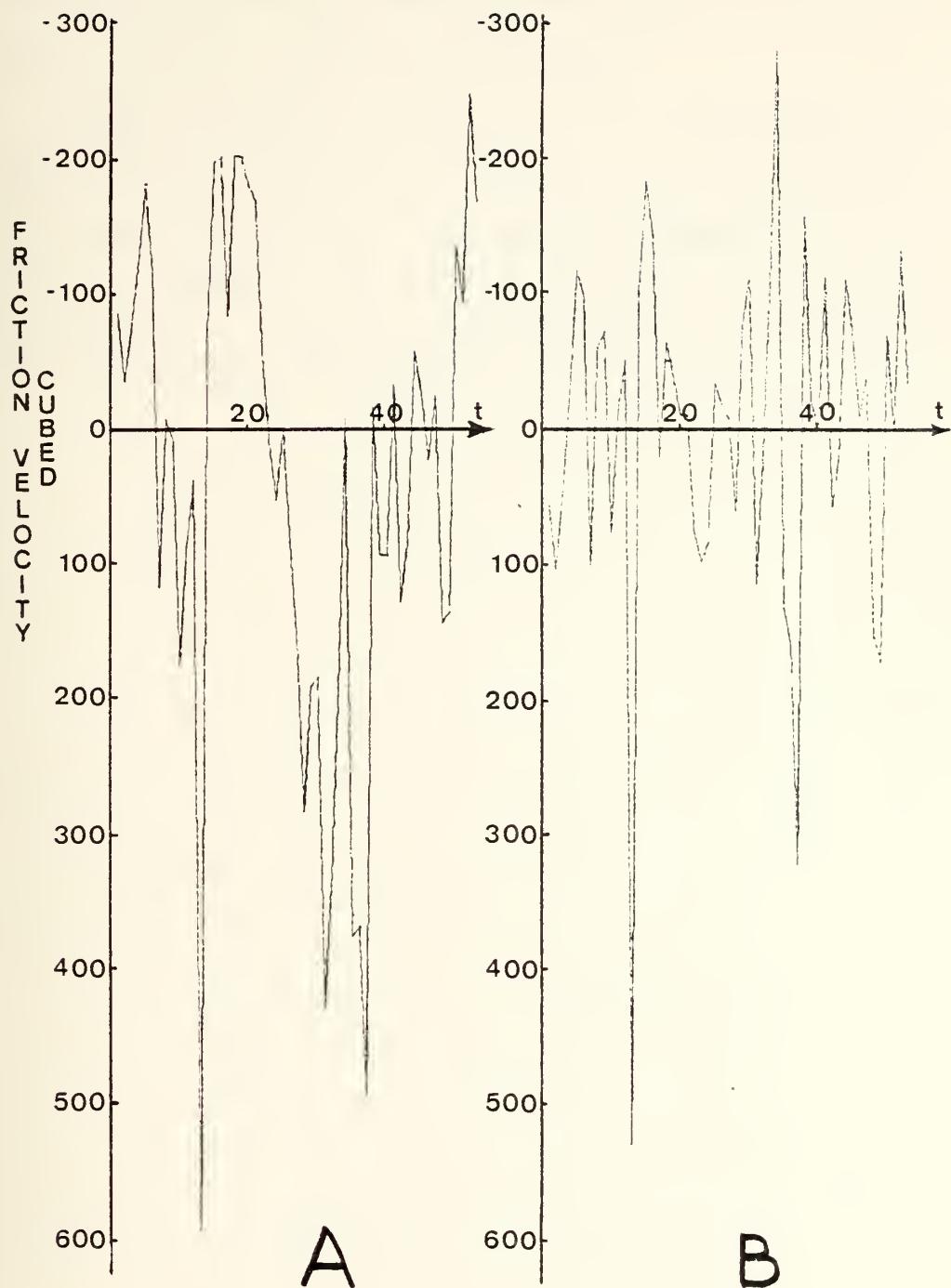
Figure 9. Weekly time (t) series for $(U_*^3)'$ for May 74 – May 75 at 32.5°N and 87.5°W (Station #3)
A. Represents the annual mean removed
B. Represents the seasonal cycle removed.

shape was obvious in the data, especially the SST. Therefore it was

necessary to remove the seasonal effect since the interest of this study

was the synoptic time scale perturbations.

Harmonic analysis of the data was done, and the mean and first

three harmonics, eliminating the seasonal cycle, were removed, leaving

the synoptic frequencies. This synoptic frequency part of the

$(\text{curl}_z \tau)'$, $(U_*^3)'$, and SST' were then plotted in time series to verify

that the seasonal effect had been removed (Figures 7B, 8B, 9B).

V. OBSERVATIONS

A. WARM SST TONGUE

A study of the sea surface temperature maps for the year period showed a very apparent tongue of warm water migrating from the North to the South near the coasts of Ecuador and Peru.

A moderately warm finger (17°C) began forming in September (Figures 10, 11, 12), sloping down from the northwest parallel to and about 5°S from the coast. It essentially remained stationary until November when it extended farther down the coast to about 20° South latitude. By the end of November the core was 18°C. At the end of December, the core warmed to 19°C and in January to 21°C. By February the maximum temperature was 23°C. The basic structure of this warm anomaly was still tongue-shaped from the North and extended to 20° South latitude. Its temperature decreased in March, and as May developed, the tongue vanished totally.

The change in temperature in this area (20°S, 75° West) was 8.4°C from 28 August 1974 (-3.8°C below mean) to 19 February 1975 (+4.6°C above mean). It would be difficult to attribute this SST difference wholly to seasonal change, or at least to the kind of seasonal change seen in neighboring areas which are notably smaller.

B. COMPARISON OF NOAA/NESS GOSSTCOMP DATA WITH THAT OF NOAA/NMFS MEAN MONTHLY SST MAPS

The products from NOAA/NESS GOSSTCOMP and NOAA/NMFS appeared somewhat similar. The NMFS usually and strong coastal gradients and North-South gradients at the equator. This was not shown on the GOSSTCOMP

30
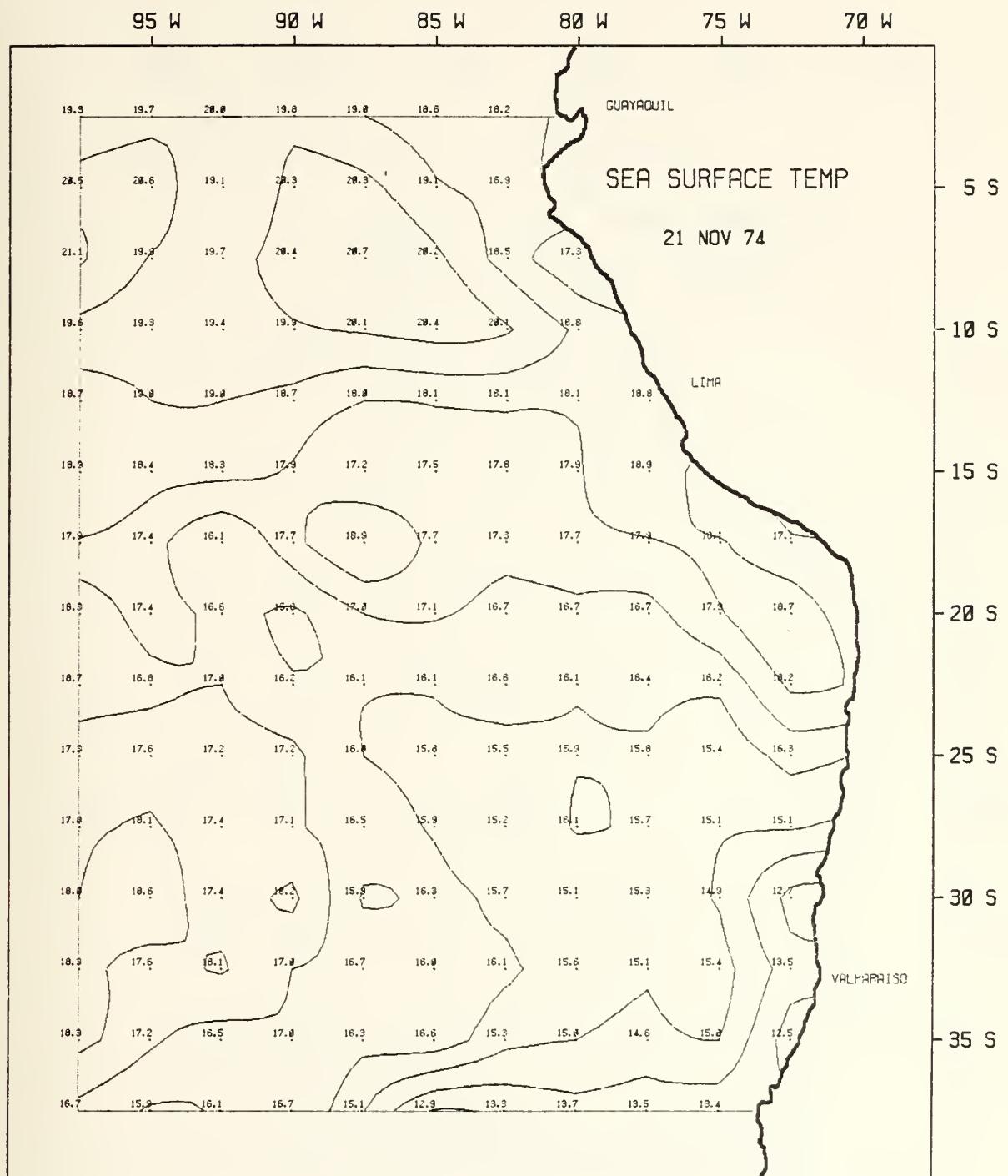
Figure 10. Sea surface temperatures (°C).

Figure II. Sea surface temperatures (°C).

32
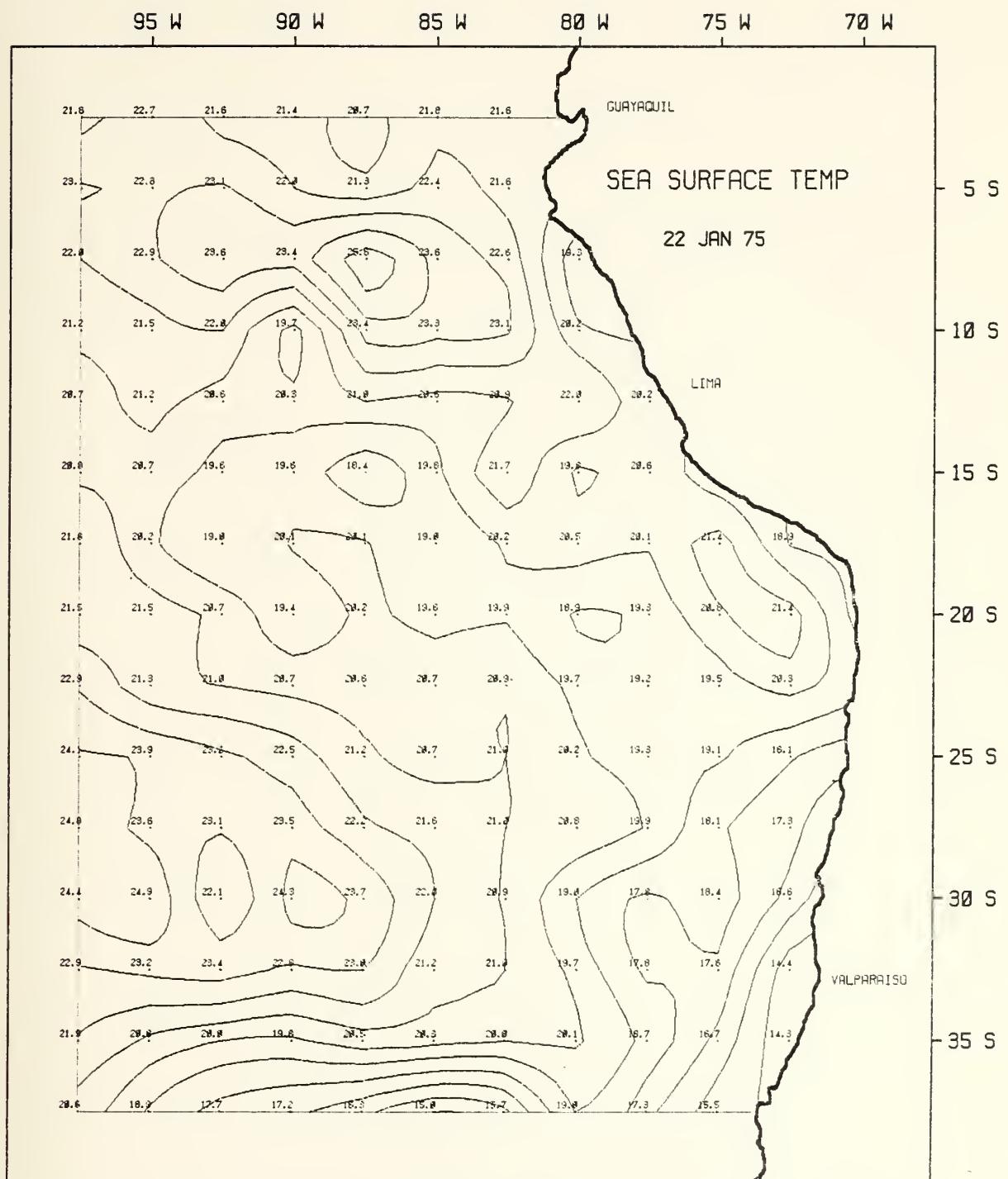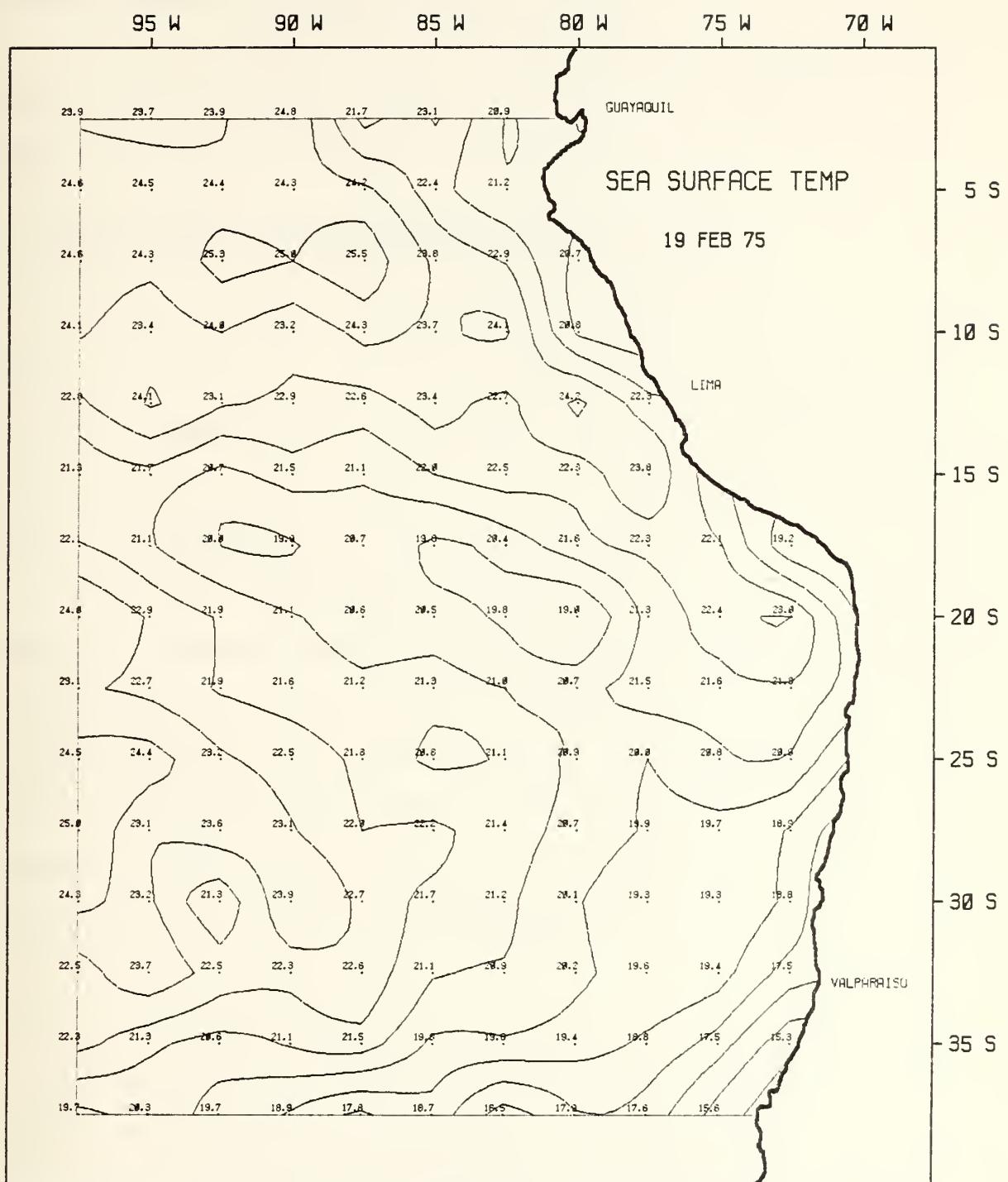
Figure 12.   Sea surface temperatures (°C).

data. Some significant anomalies were observed in May and November on both products. The basic trends in the GOSSTCOMP data were depicted in the NMFS generally, though not always consistently.

It should be pointed out that the NMFS SST maps are means and did indicate that the data was sparse in this particular region. The GOSSTCOMP was an accumulated short time daily average.

C. COMPARISON OF SMOOTHED GOSSTCOMP DATA WITH DATA
   FROM EL NINO WATCH CRUISE, 11 FEB 75 to 27 MAY 75

This shipboard data was supplied by the NMFS from the University of Hawaii and the Scripps Institution of Oceanography investigation of El Niño (reference Wyrtki, et al. 1976). Data was extracted from this investigation that corresponded the closest in space and in time to available GOSSTCOMP data in the area of interest (Table I).

Of the several random examples selected for comparison, the average absolute difference between the cruise data and GOSSTCOMP data was 1.17°C. In NOAA/NESS TM 78, the indication for 0°-360° longitude from 20° South to 90° South was a mean absolute difference in ship measurement versus satellite measurements was 0.75°C. For the purpose of this study it was assumed that SST fluctuations equal to or greater than 1°C in the GOSSTCOMP data were an accurate representation of the ocean conditions.

D. SST' AND (CURL OF TAU)'

An observation of the maps of the deviation of the means indicated a relationship of $(\text{curl}_z \tau)$ to SST'. As previously mentioned in the Southern Hemisphere with associated positive(negative) values of the $(\text{curl}_z \tau)'$, Ekman convergence (divergence) leading to surface warming (cooling) can be expected. Four cases of Ekman pumping were selected from the synoptic maps and summarized in Table II. For example,

34

	Date	Location of Mona Wave	A Mona Wave SST (°C)	GOSSTCOMP Location	B GOSSTCOMP SST (°C)	B-A ΔT(°C)
1	26 Feb 75	14.00S 93.93W	22.77	15.0S 92.5W	22.2	-0.6
2	26 Mar 75	9.00S 85.93W	27.02	10.0S 85.0W	24.5	-2.5
3	23 Apr 75	4.77S 91.20W	27.00	5.0S 90.0W	25.4	-1.6
4	23 Apr 75	2.50S 92.56W	25.85	2.5S 92.5W	25.9	0.0
5	30 Apr 75	12.54S 91.91W	24.16	12.5S 90.0W	26.0	+1.8
6	30 Apr 75	13.96S 88.97W	22.86	15.0S 87.5W	22.1	-0.9
7	7 May 75	2.49S 86.00W	23.88	2.5S 85.0W	24.7	+0.8

Average Absolute Error = 1.17°C
Average Error = -.43

Table 1. Sample of El Niño Watch (Mona Wave) data vs. GOSSTCOMP data.

35

Table 11. Summary of cases showing relationship in time between $\text{curl}_z\ \tau$ and SST'.

Case 1
30°S
90°W
(warming)

11 Sept 74		19 Sept 74		25 Sept 74	
SST'	−5.1	SST'	−3.6	SST'	−3.6
$\text{Curl}_z\ \tau$	+11.8	$\text{Curl}_z\ \tau$	+63.	$\text{Curl}_z\ \tau$	+34.8

Case 2
25°S
90°W
(warming)

06 Nov 74		13 Nov 74	
SST'	−4.3	SST'	−2.8
$\text{Curl}_z\ \tau$	+4.7	$\text{Curl}_z\ \tau$	+12.0

(Figures 13, 14, 15, 16)

Case 3
30°S
90°W
(cooling)

12 Feb 75		19 Feb 75	
SST'	+4.9	SST'	+3.5
$\text{Curl}_z\ \tau$	−2.3	$\text{Curl}_z\ \tau$	−22.5

(Figures 17, 18, 19, 20)

Case 4
35°S
80°W
(warming)

12 Mar 75		19 Mar 75		26 Mar 75	
SST'	+3.7	SST'	+4.9	SST'	+4.5
$\text{Curl}_z\ \tau$	+12.5	$\text{Curl}_z\ \tau$	+22.9	$\text{Curl}_z\ \tau$	−1.0

36

Figure 13. Sea surface temperature deviations from the mean in °C.
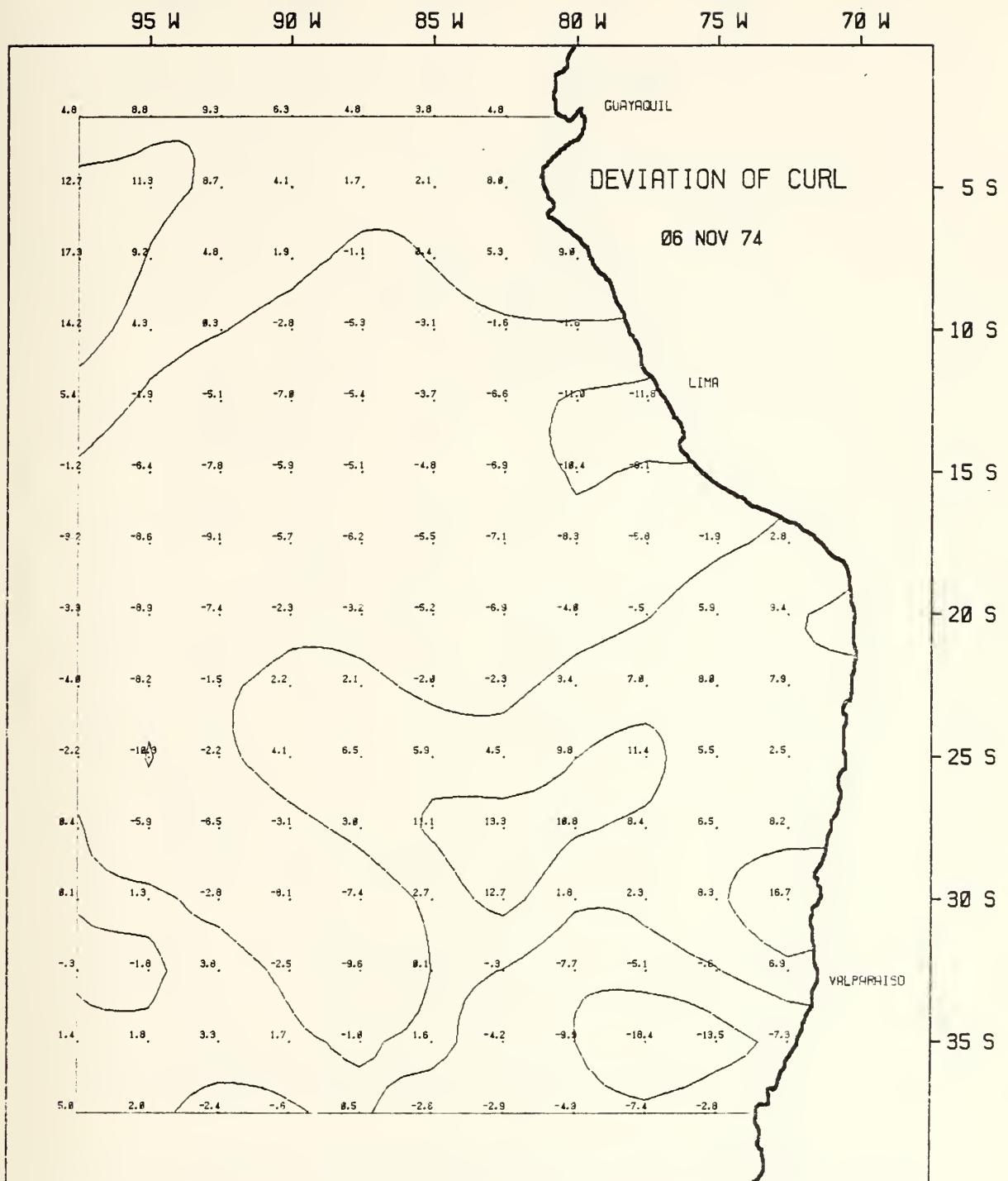
Figure 14. Deviations from the mean of $curl_z \tau$ in 10^{-9} dyne/cm^3.
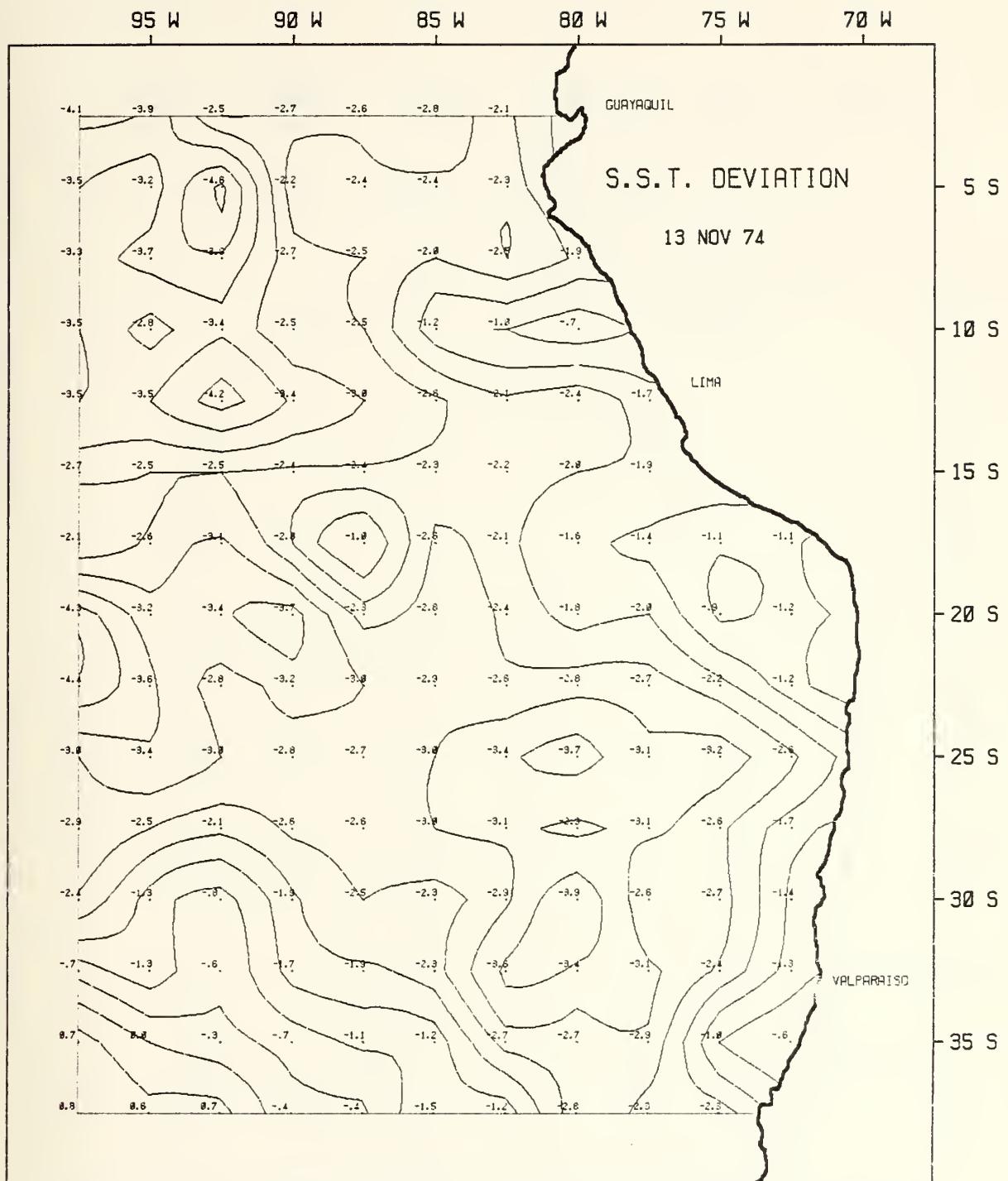
Figure 15. Sea surface temperature deviations from the mean in °C.
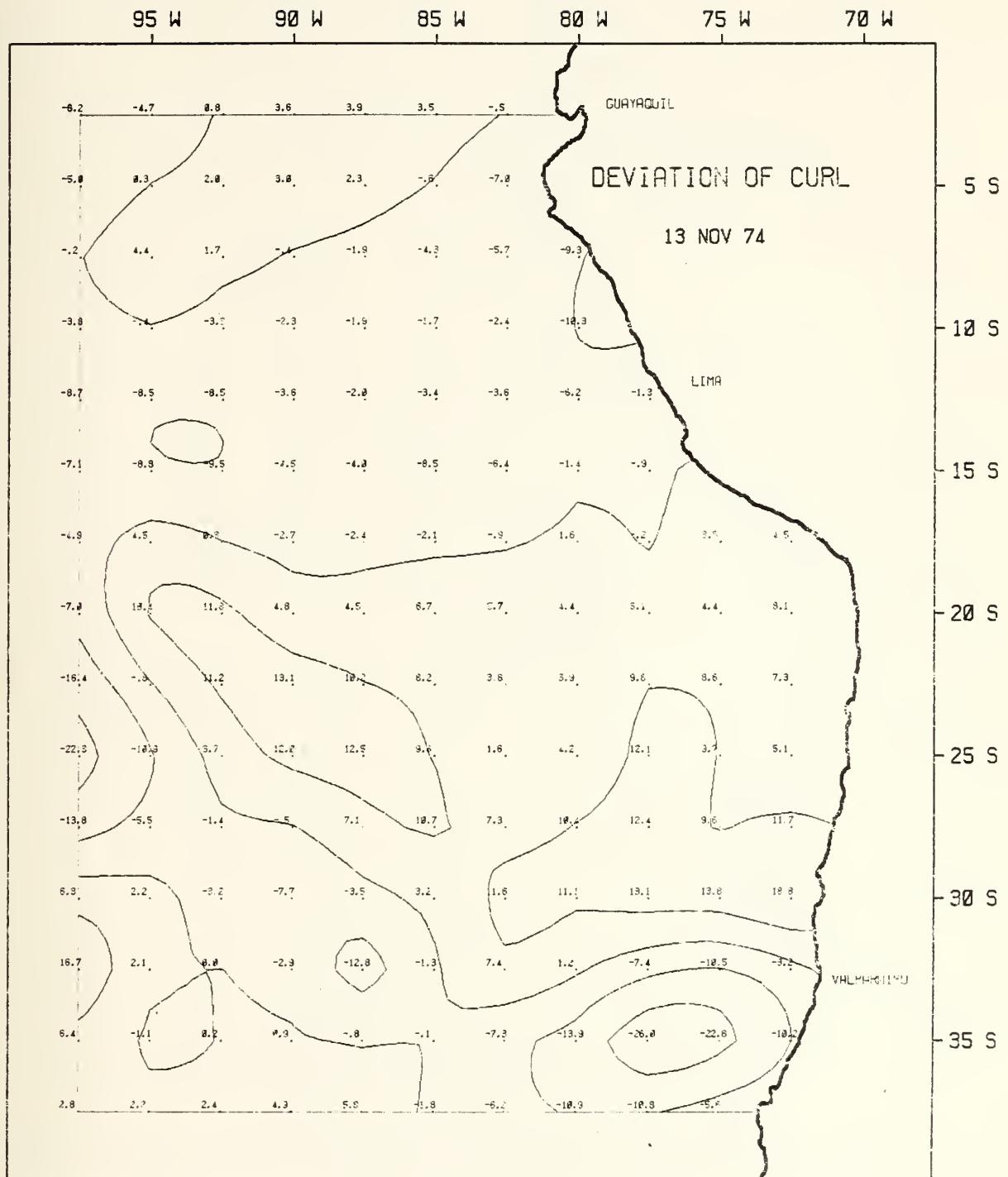
Figure 16. Deviations from the mean of curl$_z$ τ in 10^{-9} dyne/cm^3.
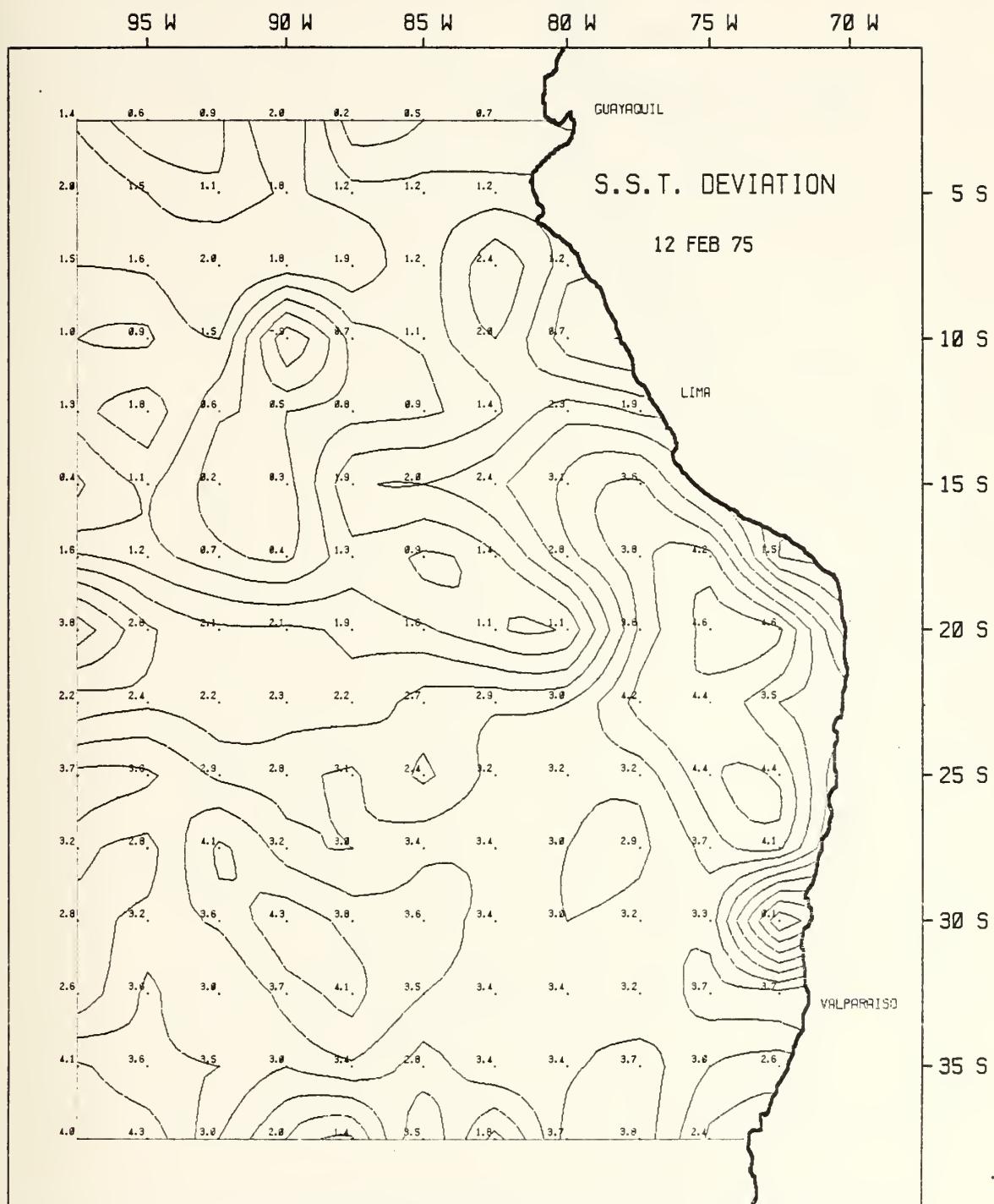
Figure 17.   Sea surface temperature deviations from the mean in °C.
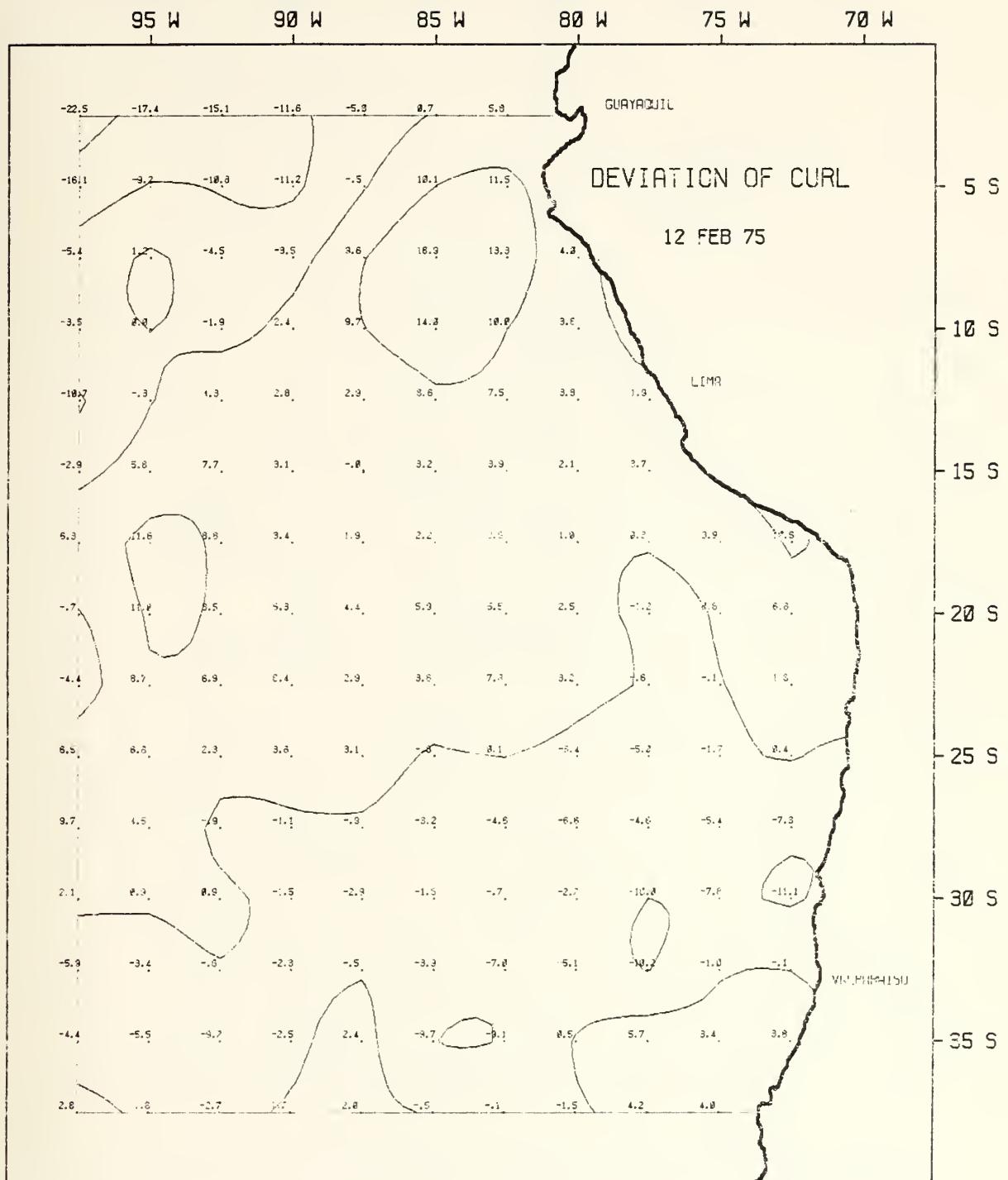
Figure 18. Deviations from the mean of $curl_z \tau$ in 10^{-9} dyne/cm^3.
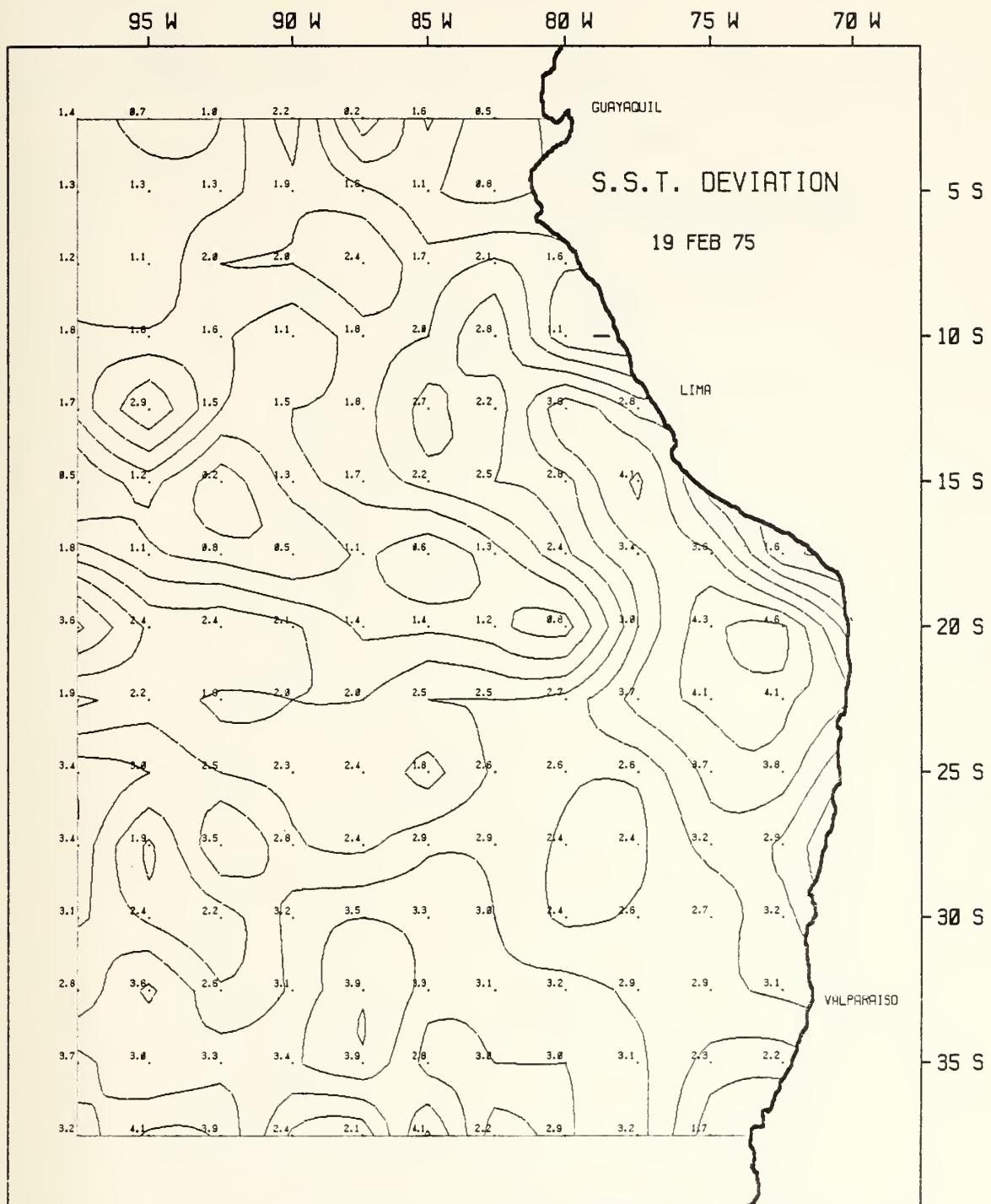
Figure 19.   Sea surface temperature deviations from the mean in °C.
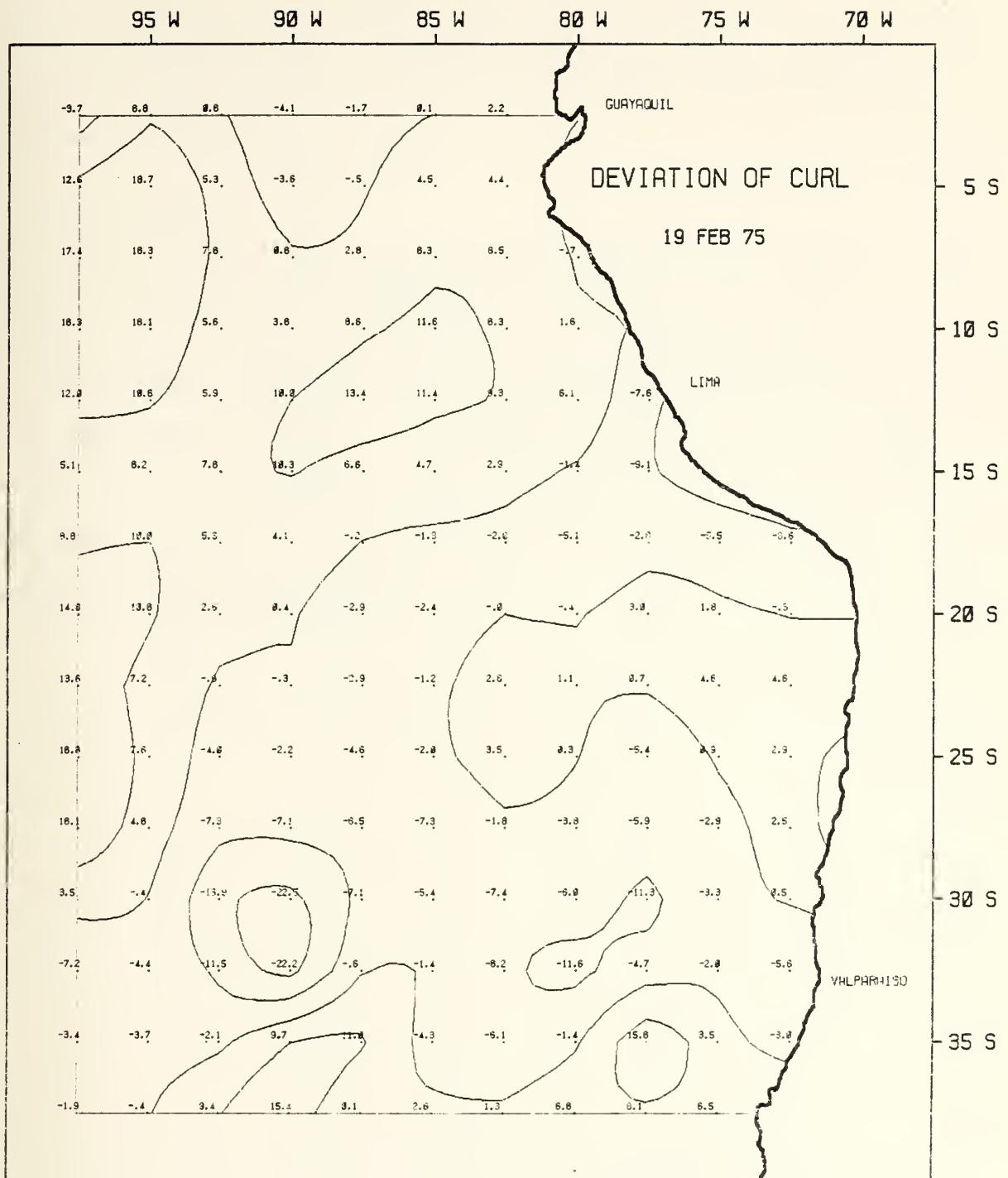
Figure 20. Deviations from the mean of curl$_z$ τ in 10^{-9} dyne/cm^3.

in Case I, at 30°S, 90°W from II September 1974, to 25 September 1974, the $curl_z \tau$ anomaly was strongly positive and the SST' increased during this time period from -5.1°C to -3.6°C. The other three cases show a similar relationship.

E. SST' AND $(U_*{}^3)'$

An examination of the anomaly maps indicated a relationship of $(U_*{}^3)'$ to SST'. As this wind increased above normal (or mean), lower values of SST' were seen. Two cases of mixing were selected from the synoptic maps and summarized in Table III. For example, in Case I at 32.5°S, 75°W from 5 June to 19 June 1974, the $U_*{}^3$ anomaly was strong and the SST' decreased during this time period from +1.6°C to -2.7°C. The other case shows a similar relationship.

.

Case I
32.5°S
75°W
(cooling)

05 June 74	12 June 74	19 June 74
SST' +1.6	SST' -1.5	SST' -2.7
(U_*^3) +101	(U_*^3) +229	(U_*^3) +83

Case 2
32.5°S
85°W
(cooling)

14 Aug 74	21 Aug 74	28 Aug 74
SST' -3.1	SST' -3.4	SST' -4.0
(U_*^3) +130	(U_*^3) +402	(U_*^3) -62

(Figures
21, 22, 23,
24, 25, 26)

Table III. Summary of two cases showing relationship in time between $(U_*^3)'$
and SST'.

46
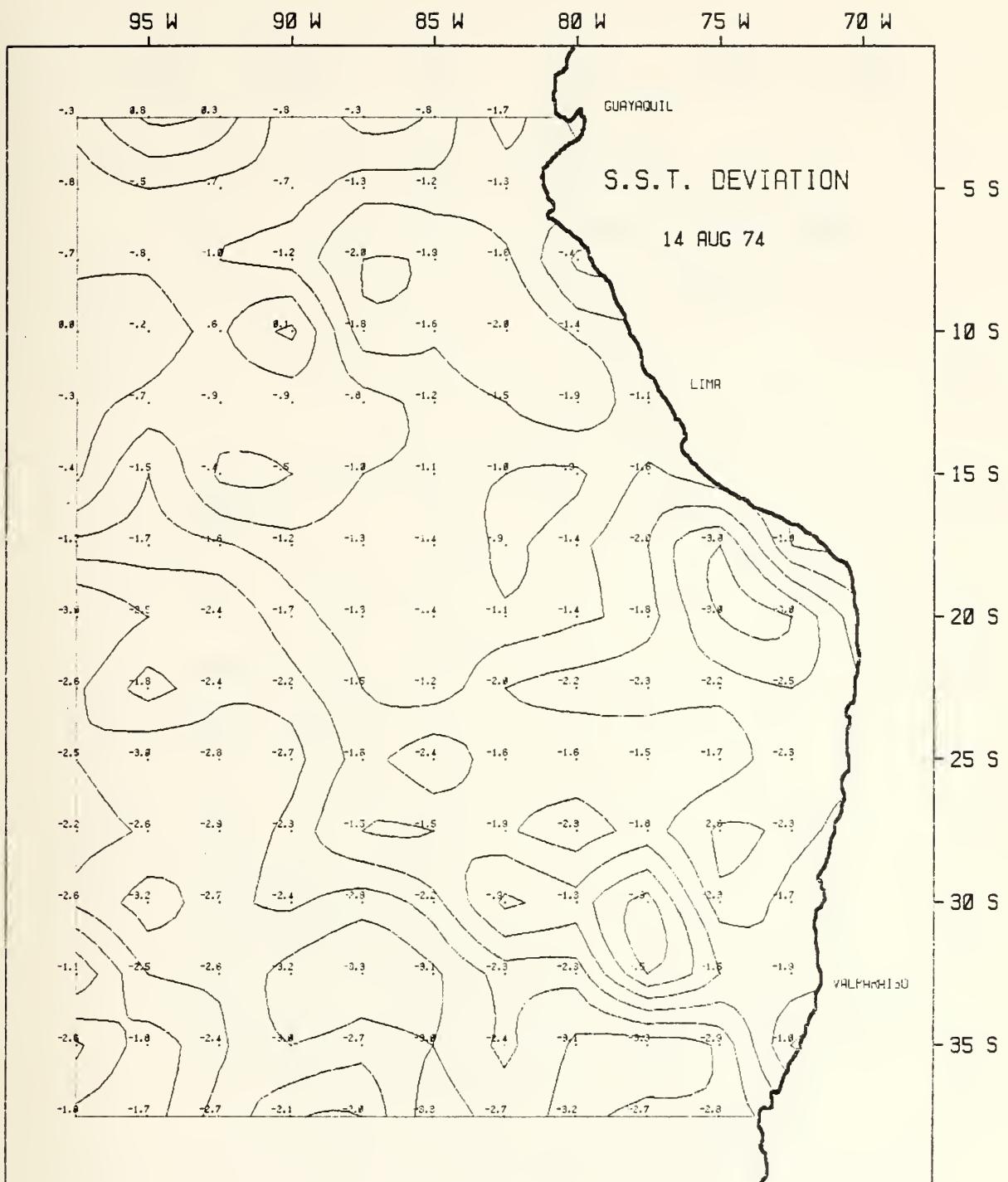
Figure 21. Sea surface temperature deviations from the mean in °C.
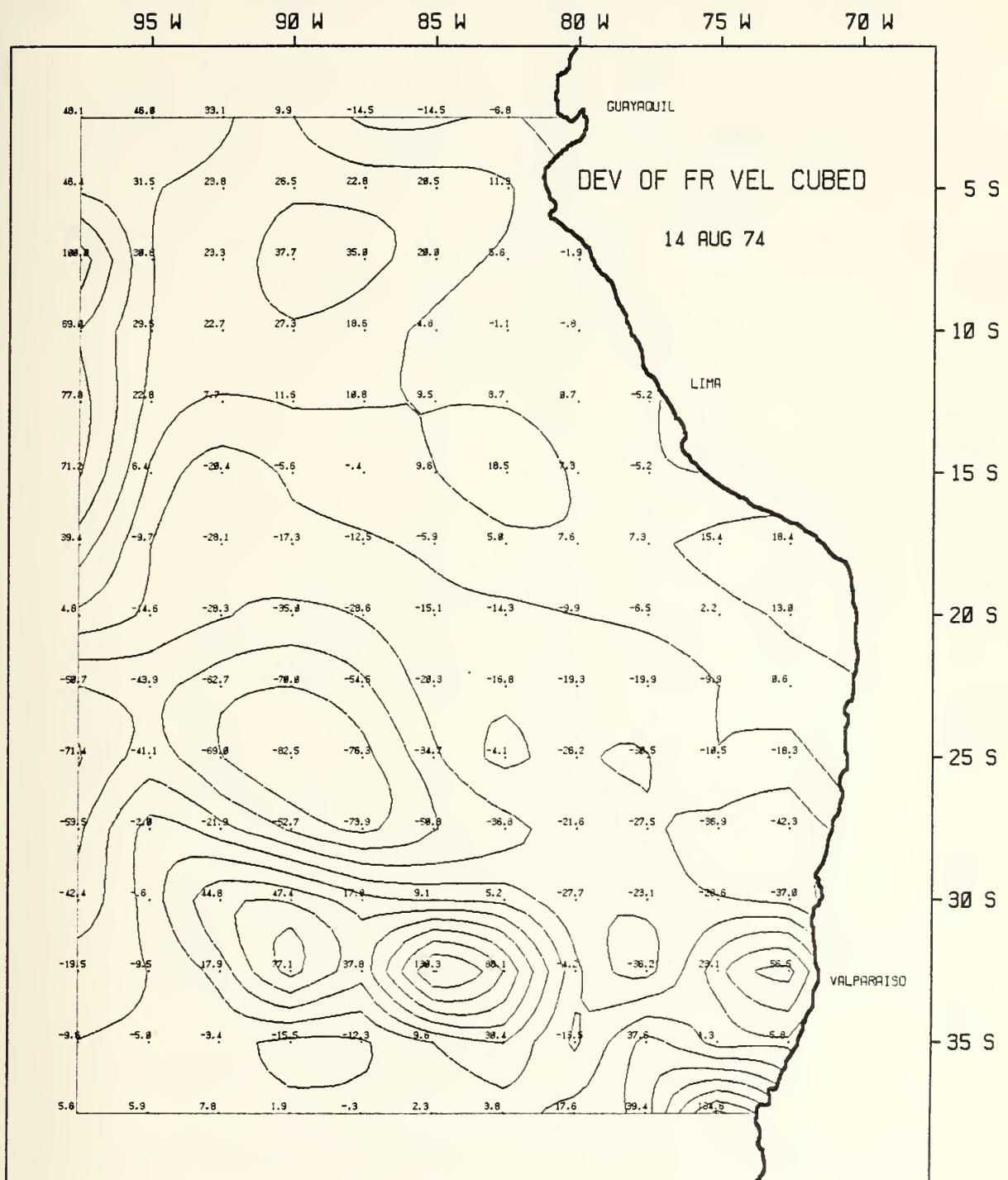
Figure 22. Deviations from the mean of U_*^3 in 10^2 cm/sec.
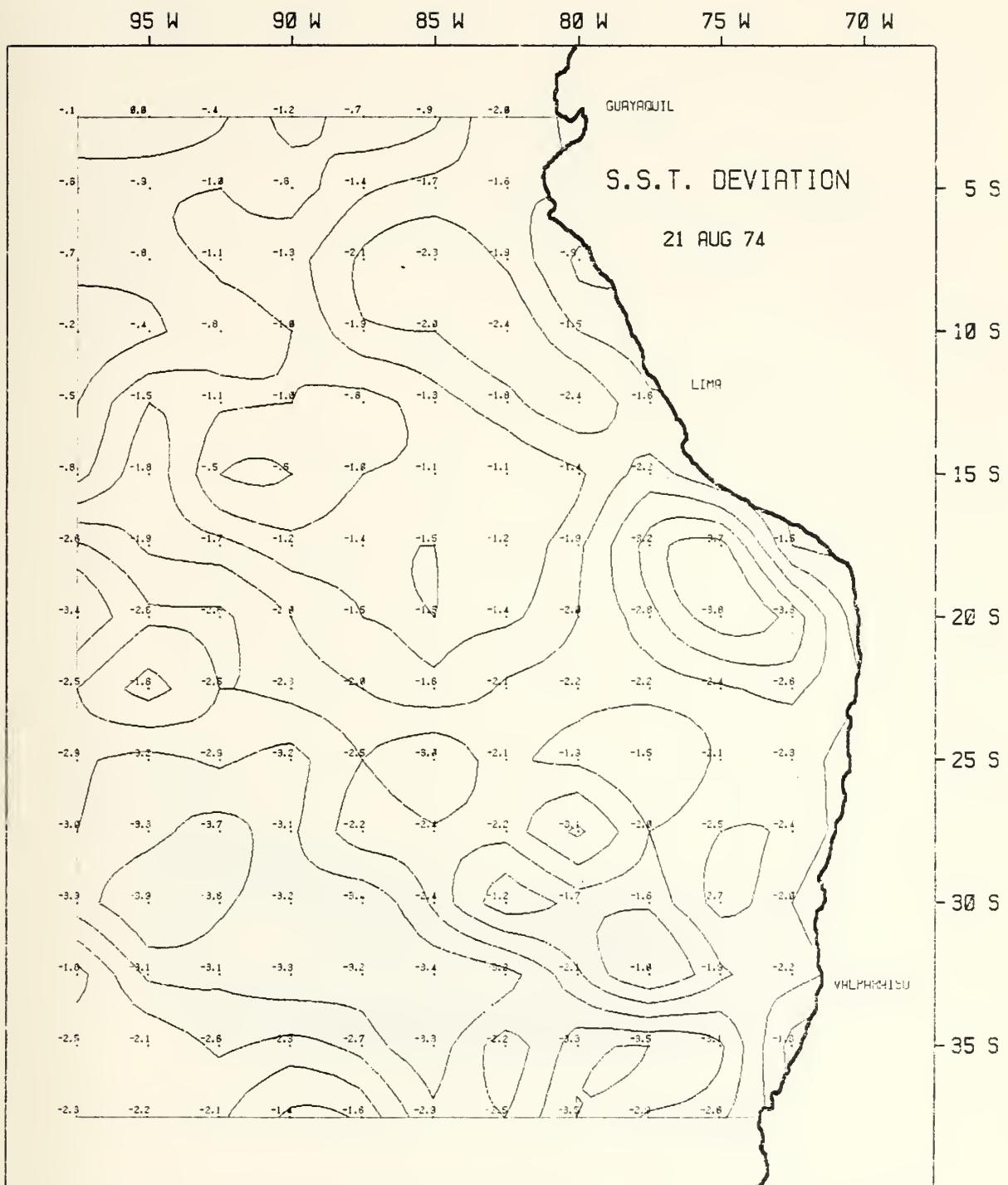
Figure 23. Sea surface temperature deviations from the mean in °C.

DEV OF FR VEL CUBED

21 AUG 74

GUAYAQUIL

LIMA

VALPARAISO
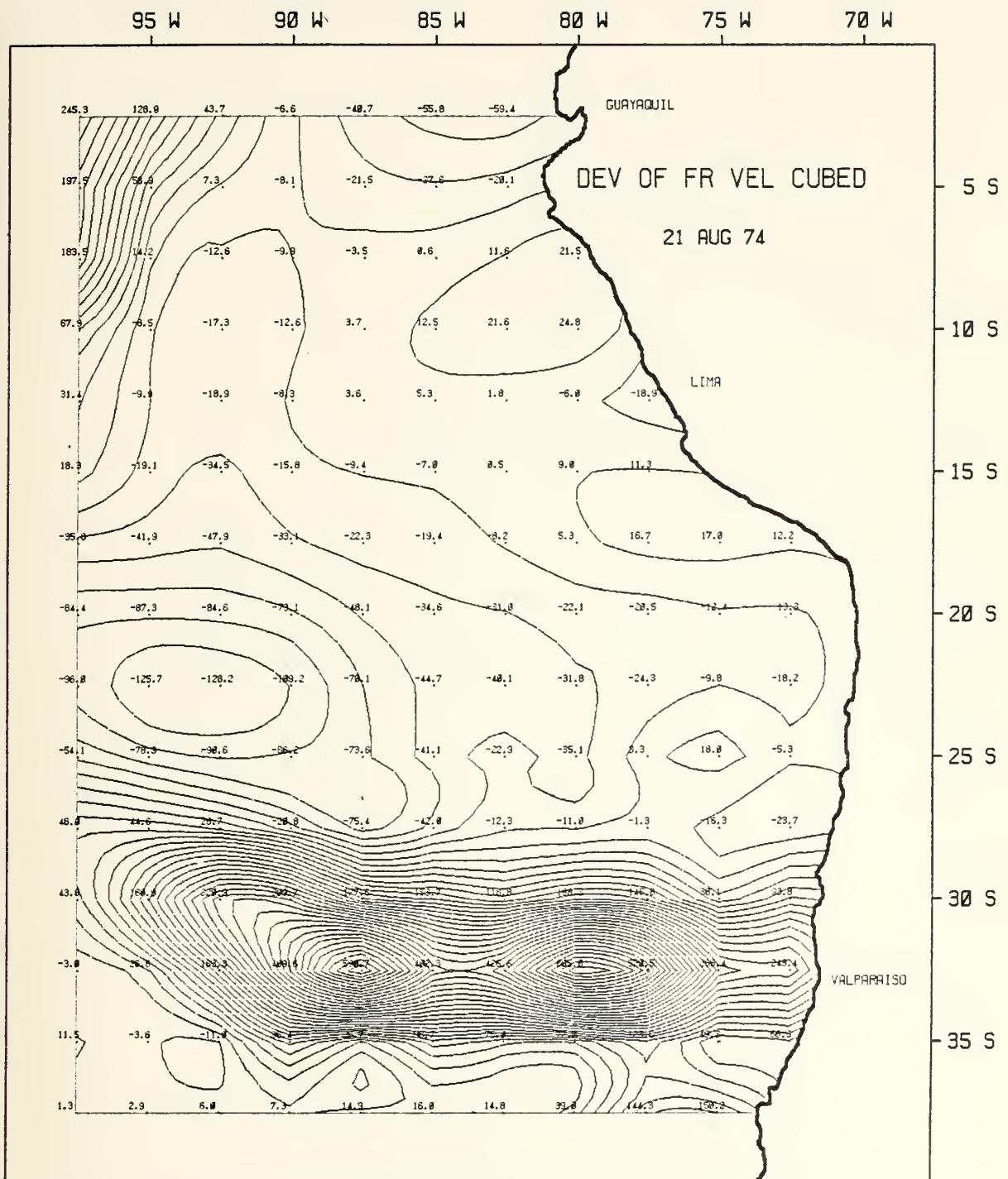
Figure 24. Deviations from the mean of U_*^3 in 10^2 cm/sec.
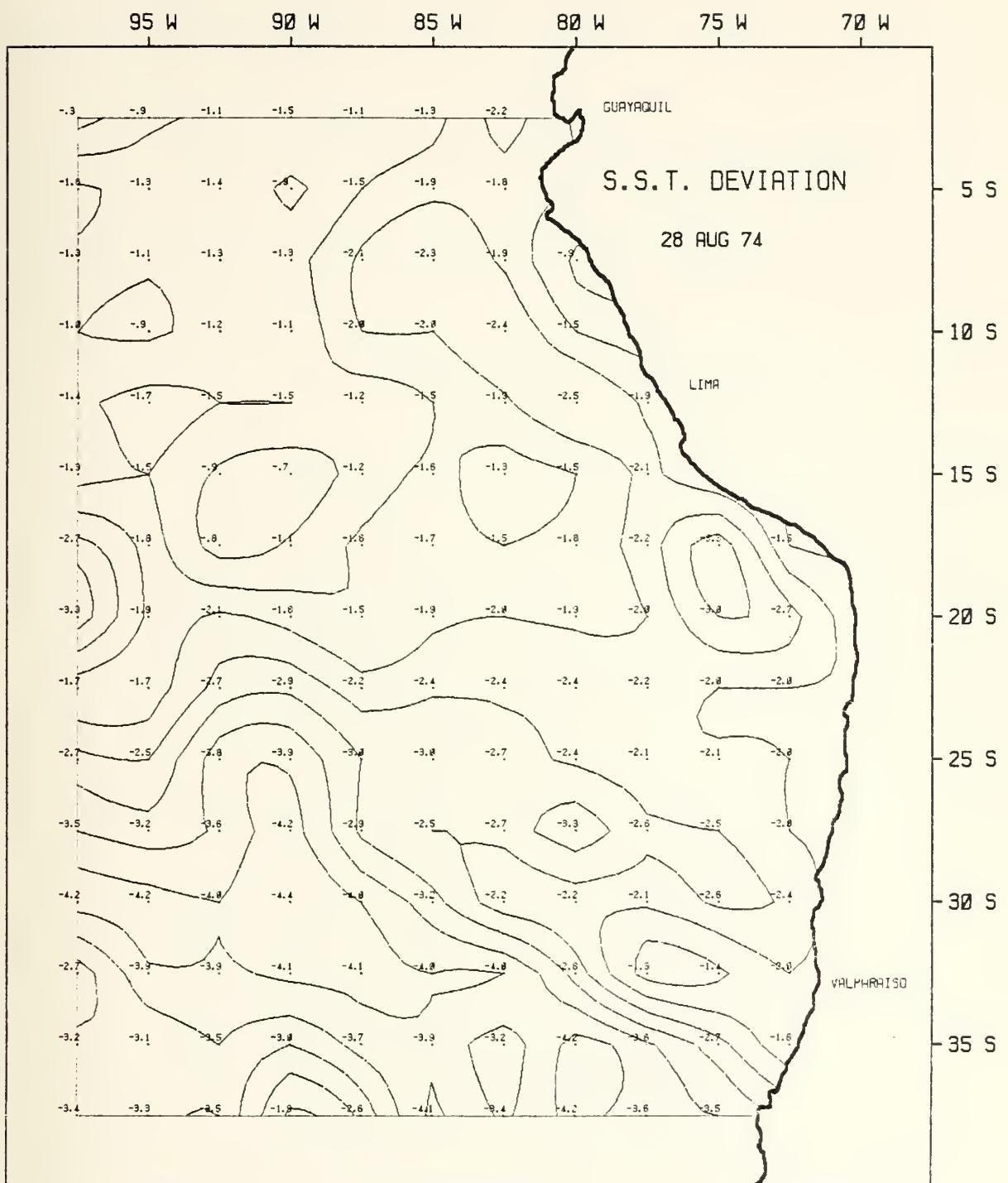
Figure 25. Sea surface temperature deviations from the mean in °C.
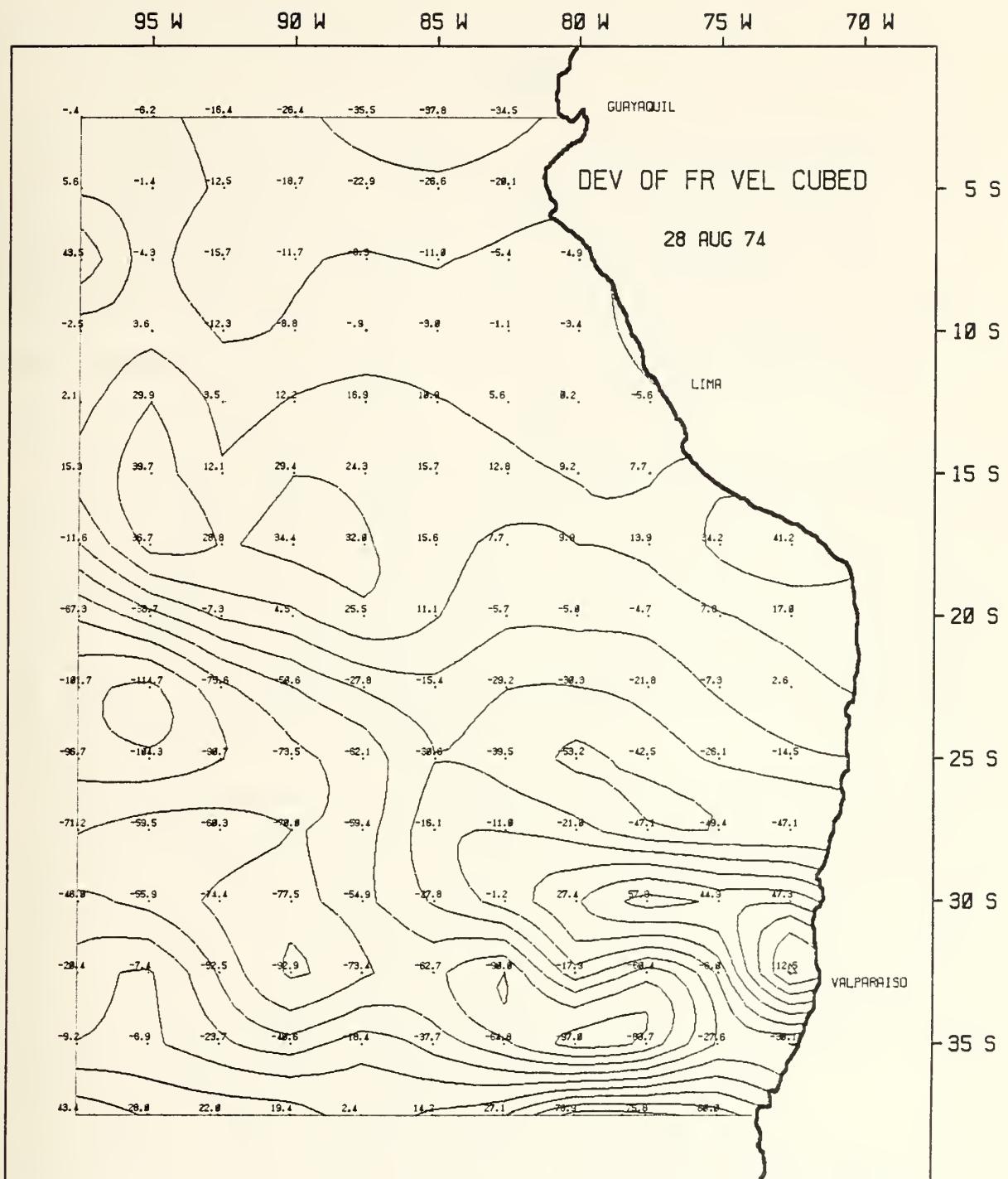
Figure 26. Deviations from the mean of U_*^3 in 10^2 cm/sec.

VI. RESULTS

To establish a statistically significant relationship between synop-
tic frequency fluctuations of SST', $(U_*{}^3)'$, and $(curl_z \tau)'$, some
types of correlation was looked for at the five points of interest
(Figure 6). The investigation points are at mid-latitudes and assumed
to be unaffected by the coast. All are at 87.5° West longitude, at
least 10° of longitude away from the coast.

Available for use in this study were Biomedical Computer Programs
from the Health Sciences Computing Facility, University of California,
Los Angeles, California, at the Computer Facility, Naval Postgraduate
School. From the P-series book, the stepwise regression program BMDP2R
was chosen. All standard statistical parameters were available along
with regression analysis and scatter plots.

Of major interest was the normalized correlation matrix (values =
0 ± 1) which showed how well the synoptic frequency parts of $(U_*{}^3)'$
and $(curl_z \tau)'$ were related to synoptic frequency parts of SST'.
Correlations r(t) were performed on these three variables with various
lags of SST' with time. One lag equalled seven days. The equations
used to correlate these variables were as follows:

11. r(SST'(t + lag) • (curl of τ)'(t))   t = time

12. $r(SST'(t + lag) \cdot (U_*{}^3)' (t))$ lag from 0 to $\pm$ 4 weeks

A lag of zero meant that the two variables were correlated at the
same time. Lags greater than (less than) zero meant that values of SST'
were compared to values of $(U_*{}^3)'$ and $(curl_z \tau)'$ in the past (future).
inally, for each lag, r(t) was averaged over the year of data giving

time average lag-correlations (Table IV). A sample of the time averaged

correlations at Stations #3 and #4 may be seen in Figures 27 and 28.

Each variable was also correlated with itself to see how rapidly the

parameter would change with time (Table V). Graphic representation of

this auto-correlation shows that the synoptic frequency oscillations in

$(U_*^3)'$ and $(curl_z \tau)'$ occurred on a shorter time scale than that of

SST' (Figure 29).

SST' LAG GRID #	-4	-3	-2	-1	0	+1	+2	+3	+4
(A) 1	+ .1294	+ .0806	- .0624	- .1123	- .0171	- .0506	- .0312	- .0135	+ .0909
(A) 2	- .1519	- .2814	- .3199	- .2671	- .1564	- .0952	+ .1938	+ .3194	+ .2877
(A) 3	- .1774	- .1774	- .1846	- .0888	- .0152	+ .1842	+ .3513	+ .2564	+ .0543
(A) 4	- .1323	+ .2113	+ .5295	+ .2724	+ .3706	+ .1667	- .1216	- .0884	- .3165
(A) 5	- .0443	+ .2712	+ .2325	+ .1783	+ .1026	- .0044	+ .0489	- .2373	- .2594
(B) 1	+ .1608	- .0020	+ .0199	- .1460	- .1234	- .1343	+ .1335	+ .0411	+ .0102
(B) 2	+ .0129	+ .1262	+ .0705	- .0541	- .0753	- .0838	+ .0296	- .1307	- .0377
(B) 3	+ .2542	+ .3251	+ .2854	+ .0510	+ .1206	- .0634	- .2495	- .2758	- .1132
(B) 4	- .0055	+ .0099	+ .2564	+ .0259	+ .1845	- .0124	- .0376	+ .0198	+ .0175
(B) 5	+ .2316	+ .0512	+ .1031	- .0085	- .1192	+ .0783	- .0691	- .0808	- .0752

Table IV. Time averaged lag correlations between SST' and curl$_z$ τ'(A) and (U_*^3)'(B) at the five selected grid points. A positive lag means SST' is evaluated at the advanced time. Each lag corresponds to seven days.

55
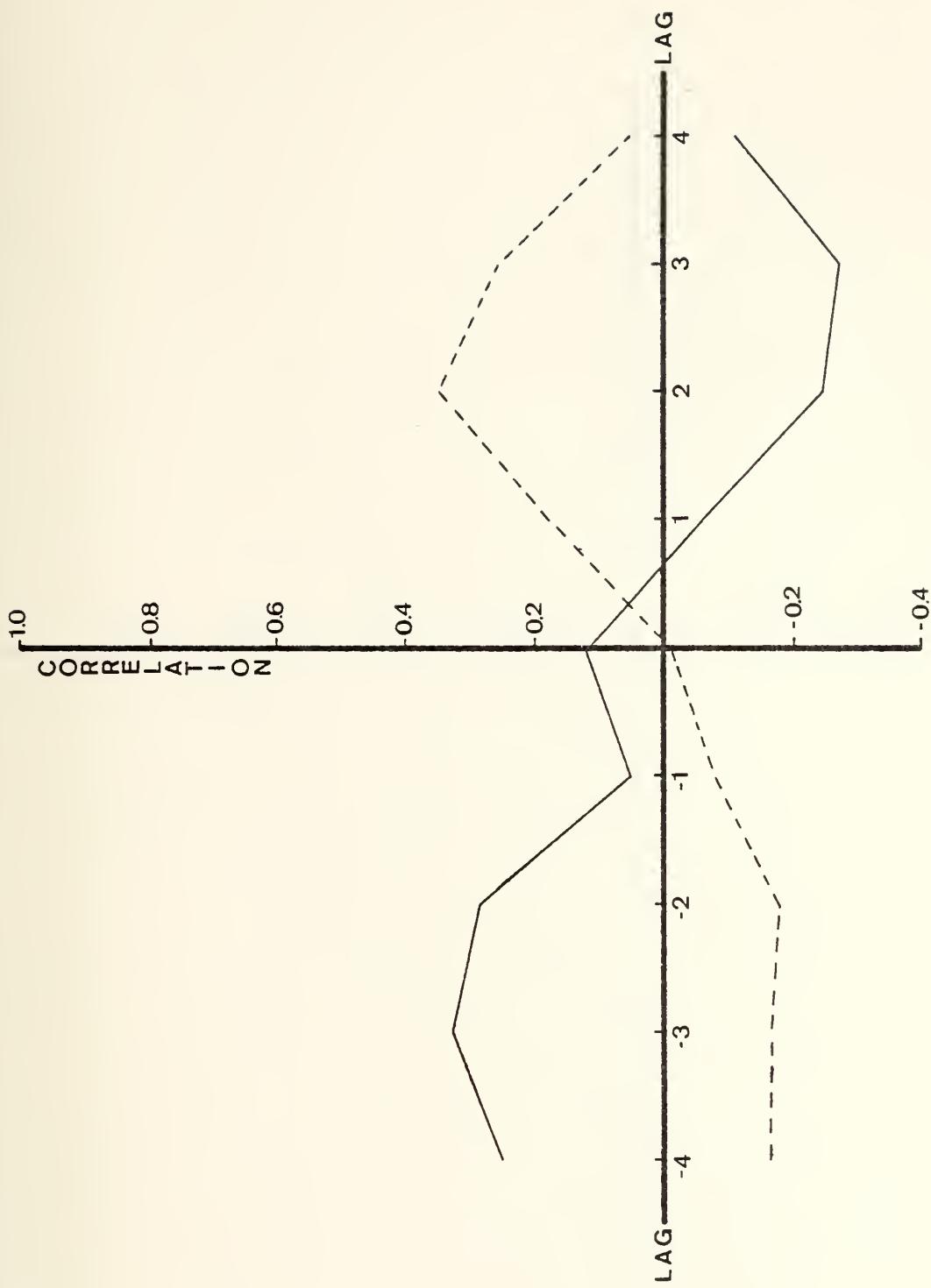
Figure 27. At Station #3 time averaged correlation of SST' with $(U_*^3)'$ as a function of lag (——) Time averaged correlation of SST' with $(curl_z \tau)'$ as a function of lag (– – –). Refer to equations 11 and 12.
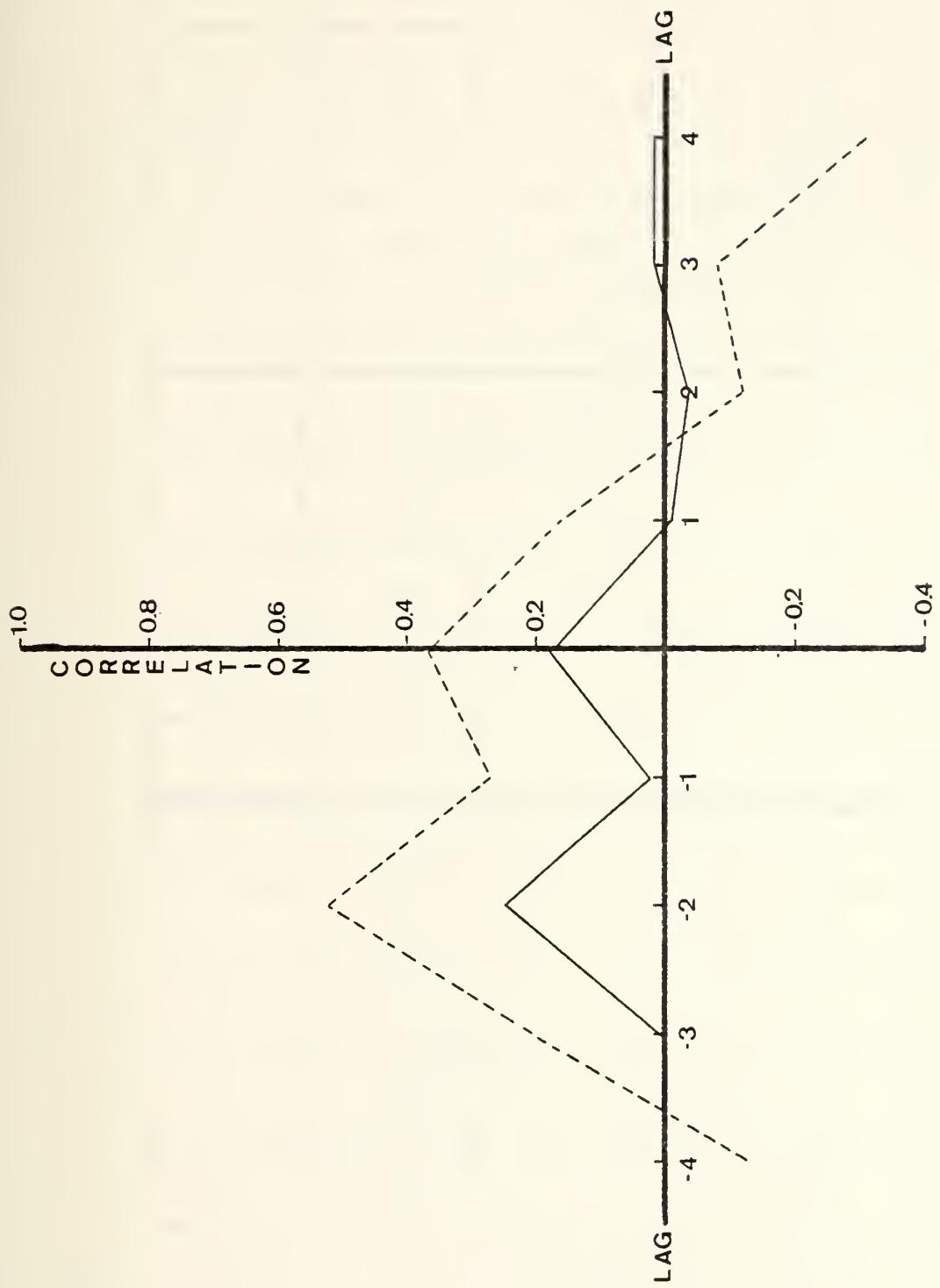
Figure 28. At Station #4 correlation of SST' with $(U_*{}^3)'$ as a function of lag (——)
Correlation of SST' with $(\text{curl}_z \ \tau)'$ as a function of lag (---). Refer to
equations 11 and 12.

LAG → STA# ↓	0	±1	±2	+3	+4	
1	1.00	+ .4244	+ .0251	− .3017	− .3616	
2	1.00	+ .5425	+ .2573	− .1191	− .3412	
3	1.00	+ .5064	+ .1412	− .1069	− .2553	A
4	1.00	+ .4470	+ .1240	− .1115	− .3219	
5	1.00	+ .1062	− .1478	− .0713	− .1890	
1	1.00	− .1726	− .1584	− .2269	− .1332	
2	1.00	+ .0116	+ .0308	− .1802	− .3101	
3	1.00	+ .1996	− .3881	− .3712	+ .1014	B
4	1.00	+ .1974	− .0791	− .0791	− .2901	
5	1.00	− .0316	− .0761	+ .1739	− .3266	
1	1.00	− .0630	+ .1411	− .0847	− .2870	
2	1.00	− .0920	− .2413	− .2225	+ .0410	
3	1.00	+ .0057	− .2400	− .1871	− .0561	C
4	1.00	− .3506	− .0474	+ .0843	− .2394	
5	1.00	− .0747	− .1577	− .1860	− .1888	

Table V. Autocorrelation values for SST'(A), $\text{curl}_z \tau'$(B), $(U_*^3)'$(C).

VII. CONCLUSIONS

The correlation values were not what were expected. The highest correlation (+.5293) for $(curl_z \tau)'$ occurred at a -2 week lag of SST' at point #4, and the highest correlation (+.3251) for $(U_*^3)'$ occurred at a -3 week lag of SST' at point #3; but these results can be given little weight since they are not part of a coherent pattern in the correlation matrix.

The basic theory was that the curl of Tau when positive would produce surface Ekman convergence of ocean waters with downwelling causing warming (weak effect) of the sea surface. When the curl of Tau was negative, the surface Ekman divergence should come with upwelling and cooling (strong effect) of the sea surface. Thus the time average correlations between SST' and $(curl_z \tau)'$ was expected to be positive at positive lags. High surface friction wind (U_*) should cause surface mixing resulting in cooling. Thus SST' and $(U_*^3)'$ should be negatively correlated at positive lag.

In terms of having the "correct" sign of the correlations, station #3 came closest to the theoretical expectations in both the fields. If the data were perfect and could be completely trusted, it would appear that both processes, wind mixing and Ekman pumping, were occurring with approximately equal importance at the station. Qualitatively, about half the variance in non-seasonal SST fluctuations at two week periods would be properly related to these two processes. Unfortunately the results are not similar at the other locations (Table IV). In this study therefore, this basic theory was not supported by results.

The best explanation for the discrepancy between data and theory was that the Southern Hemisphere lacks a stable data base. Figure 7B, SST deviations with the seasonal cycle removed, showed SST' amplitudes ranging from 0 to ± 1.5°C. In Table I, Section V.C, where GOSSTCOMP data was compared to ship board data, the average absolute error between that of cruise data and GOSSTCOMP data was 1.17°C. Since the error was the same order of magnitude as the deviations, it was expected that these errors strongly influenced the SST deviations. There was no way in this report to verify FNWC's marine global band fields over the Pacific Ocean in the Southern Hemisphere. There were very few ocean observations in this region so there is a possibility of non-negligible errors in the surface wind fields as well. Thus, during the period of this study, the Southern Hemisphere products are of questionable accuracy.

The number of ships in the South Pacific Ocean reporting SST values, a prime source for checking satellite observations in the GOSSTCOMP routine, was definitely low compared to that of the North Pacific. It was also pertinent that there was a scarcity of weather observation platforms that fed data into FNWC from this very large region. Yet, even at present, these were the best available sources for study of the phenomena in the Eastern Pacific Ocean in the Southern Hemisphere.

The author strongly recommends that further investigation into this area be encouraged. More research in the Eastern South Pacific would provide a broader study base to facilitate a better understanding of the changes in this region's ocean temperatures.

LIST OF REFERENCES

BIOMEDICAL COMPUTER PROGRAMS
    1975. BMDP2R - Stepwise Regression, Health Sciences Computing
    Facility, Program revised Feb. 76, W. J. Dixon, ed., University
    of California Press, Los Angeles.

BROWER, R. L., GOHRBAND, H. S., PICHEL, W. G., SIGNORE, T. L., WALTON,
    C. C., 1976. Satellite Derived Sea Surface Temperatures from
    NOAA Spacecraft, NOAA/NESS Technical Memorandum #78, Washington,
    D. C.

EL NINO WATCH--UNDERWAY PROGRAM
    1976. Thermosalinograph Data and XBT Log, 11 Feb 1975, to 27 May
    1975, Data report prepared by GEOSECS Operations Group/NSF, A. E.
    Bainbridge, Project Director, R/V MONAWAVE, University of Hawaii.

FISHING INFORMATION
    May 1974 #5; June 1974 #6; July 1974 #7; August 1974 #8; September
    1974 #9; October 1974 #10; November 1974 #11, December 1974 #12;
    January 1975 #1; February 1975 #2; March 1975 #3; April 1974 #4;
    May 1975 #5; U. S. Department of Commerce, NOAA, National Marine
    Fisheries Service, Southwest Fisheries Center, La Jolla, California.

GLOSSARY OF METEOROLOGY
    1959. R. E. Huschke, ed., American Meteorological Society, Boston,
    Mass.

HANTEL, M.
    1970. Monthly charts of surface wind stress curl over the Indian
    Ocean, Monthly Weather Review, V 98.

NELSON, C. S.
    1976. Wind stress and wind stress curl over the California Current,
    M.S. Thesis in Oceanography, Naval Postgraduate School, Monterey,
    California.

WYRTKI, K., STROUP, E., PATZERT, W., WILLIAMS, R., QUINN W.
    1976. Predicting and Observing El Nino, Science, V 191, #4225.

INITIAL DISTRIBUTION LIST

No. Copies

1. Department of Oceanography, Code 68   3
    Naval Postgraduate School
    Monterey, California 93940

2. Oceanographer of the Navy   1
    Hoffman Building No. 2
    200 Stovall Street
    Alexandria, Virginia 22332

3. Office of Naval Research   1
    Code 410
    NORDA, NSTL
    Bay St. Louis, Mississippi 39520

4. Dr. Robert E. Stevenson   1
    Scientific Liaison Office, ONR
    Scripps Institution of Oceanography
    La Jolla, California 92037

5. Library, Code 3330   1
    Naval Oceanographic Office
    Washington, D. C. 20373

6. SIO Library   1
    University of California, San Diego
    P. O. Box 2367
    La Jolla, California 92037

7. Department of Oceanography Library   1
    University of Washington
    Seattle, Washington 98105

8. Department of Oceanography Library   1
    Oregon State University
    Corvallis, Oregon 97331

9. Commanding Officer   1
    Fleet Numerical Weather Central
    Monterey, California 93940

10. Commanding Officer   1
    Naval Environmental Prediction Research Facility
    Monterey, California 93940

11. Department of the Navy   1
    Commander Oceanographic System Pacific
    Box 1390
    FPO San Francisco 96610

12. Defense Documentation Center   2
    Cameron Station
    Alexandria, Virginia 22314

13. Library (Code 0142)   2
    Naval Postgraduate School
    Monterey, California 93940

14. Director   1
    Naval Oceanography and Meteorology
    National Space Technology Laboratories
    Bay St. Louis, Mississippi 39520

15. NORDA   1
    Bay St. Louis, Mississippi 39520

16. Prof. R. L. Haney, Code 63Hy   2
    Department of Meteorology
    Naval Postgraduate School
    Monterey, California 93940

17. Prof. G. J. Haltiner, Chairman   1
    Department of Meteorology
    Naval Postgraduate School
    Monterey, California 93940

18. Meteorology Department Code 63 Library   1
    Naval Postgraduate School
    Monterey, California 93940

19. Defense Mapping Agency   4
    Inter-American Geodetic Survey
    Drawer 934
    Fort Clayton, Canal Zone

20. Assoc. Prof. J. B. Wickham, Code 68Wk   2
    Department of Oceanography
    Naval Postgraduate School
    Monterey, California 93940

21. Prof. Klaus Wyrtki   1
    Department of Oceanography
    University of Hawaii
    Honolulu, Hawaii 96822

22. Dr. Robert L. Bernstein   1
    Scripps Institution of Oceanography
    La Jolla, California 92037

23. Lt. George H. Berry |
    100 Brownell Circle
    Monterey, California   93940

24. Lt. Craig S. Nelson |
    Pacific Environmental Group
    National Marine Fisheries Service
    c/o Fleet Numerical Weather Central
    Monterey, California   93940

25. Dr. Alan E. Strong, Oceanographer |
    Environmental Sciences Group
    U. S. Department of Commerce
    National Oceanic and Atmospheric Administration
    National Environmental Satellite Service
    Washington, D. C.   20233

26. Dr. Paul McClain |
    Environmental Sciences Group
    U. S. Department of Commerce
    National Oceanic and Atmospheric Administration
    National Environmental Satellite Service
    Washington, D. C.   20233

27. Defense Mapping Agency |
    Hydrographic Center
    Technical Library, Code LAL
    Washington, D. C.   20390